2020

Gain Enhancement of On-Chip Wireless interconnects at 60 GHz Using an Artificial Magnetic Conductor

Douglas Bean
dab3710@rit.edu

Gain Enhancement of On-Chip Wireless interconnects at 60 GHz Using an Artificial Magnetic Conductor

by

Douglas Bean

Thesis Submitted

in

Partial Fulfillment of the

Requirements for the Degree of

MASTER OF SCIENCE IN ELECTRICAL ENGINEERING

Approved by:

Professor _____
(Dr. Jayanti Venkataraman – Advisor)

Professor _____
(Dr. Amlan Ganguly – Committee Member)

Professor _____
(Dr. Panos Markopoulos – Committee Member)

Professor _____
(Dr. Sohail Dianat – Department Head)

DEPARTMENT OF ELECTRICAL AND MICROELECTRONIC ENGINEERING
KATE GLEASON COLLEGE OF ENGINEERING
ROCHESTER INSTITUTE OF TECHNOLOGY
ROCHESTER, NEW YORK

Publication from Present Work

Bean D., Venkataraman J., and Ganguly A. “Gain Enhancement of On-Chip Antenna at 60 GHz Using an Artificial Magnetic Conductor”, *2020 IEEE Intl Symposium on Antennas and Propagation & USNC/URSI National Radio Science Meeting*, Montreal, Canada, July 5-10, 2020 (accepted).

Abstract

The motivation for this work comes from the increased demand for short range high frequency data communication within and between integrated circuit (IC) chips. The use of wireless interconnects introduces flexibility to the circuit design, reduces power consumption and production costs, since the antennas can be integrated into a standard CMOS process. These findings have been well noted in literature. In addition, wireless interconnects operating in the mm-wave frequency range, at 60GHz, allow for a high data rate of over 1Gb/s for short range of transmissions. The drawback of wireless interconnects operating at high frequencies is the distortion in the radiation pattern caused by the silicon substrate inherent in a standard CMOS process. The high permittivity and a low resistivity of silicon in a CMOS process introduce radiation losses. These losses distort the radiating signal, reducing the directive gain and the antenna efficiency.

The objective of the work is to enhance antenna gain and improve the radiation efficiency with the use of a Jerusalem-Cross Artificial Magnetic Conductor (AMC). The Jerusalem Cross AMC can mitigate the effects of the silicon and improve data transmission for inter-Chip data communications. A Yagi antenna was optimized for end-fire radiation in the plane of the chip. It's performance was studied when it was placed in the center and along the front edge of a standard 10mm by 10mm chip, with the AMC layer extending only below the feed system, *Partial AMC*, and then compared when it extends under the entire antenna, *Full AMC*. To examine the transmission characteristics two chips were placed facing one another, on an FR4 slab, with the antennas first placed at the front edges of both chips then in the center of their respective chips. For direct comparison a third

configuration was made with one antenna in the center of a chip and the other at the edge of the second chip. The performance of this inter-chip transmission was examined with the three AMC layer configurations: *No AMC, Partial AMC,* and *Full AMC.* All simulations were performed using ANSYS HFSS.

The results show that the partial AMC improves the performance of the Yagi antenna when it was placed at the front edge of the chip facing out. The directive gain (Endfire direction) with the partial AMC was increased by 0.79 dB or 46% when compared to the antenna without an AMC. The radiation efficiency increased from 39% to 45%. When examining the antenna in the center of the larger substrate the full AMC layer improved performance. The directive gain increased by 0.93 dB or 5%. The full AMC layer improved the directional gain of the antenna in the center of the chip because it is more susceptible to the effects of the silicon substrate. Whereas when placed at the edge of the chip the antenna is mainly radiating in free space and not as influenced by the losses due to the silicon. Which is why the partial AMC improves radiation performance for the antenna placed at the edge of the chip. This is more clearly shown by the transmission results. When both antennas were placed at the front edges of their respective chips with full AMC layers the gain increased by 11% and the radiation efficiency increases by 12%; while when both antennas are placed in the center the directive gain increases by 26% and the radiation efficiency increases by only 2%. In the model with one antenna at the front edge of the first chip and the other antenna in the center of the second chip the full AMC improved the directive gain by 12% and 29% respectively. Both results show that the full AMC has a positive effect on the directive gain of the antenna, especially when placed in the center of the substrate.

Table of Contents

List of Figures

1 Introduction

1.1 Conventional Chip Communication Methods

Wired interconnects have been the dominant method for communication within and between CMOS chips. The technology in computer processors and integrated circuits (ICs) has continually gotten smaller and smaller. This shrinking has decreased the signal integrity for wired interconnects. Specifically, there are issues with crosstalk, dispersion, parasitic inductance, stray capacitance, signal delay, timing errors, and power efficiency [1]. As the ICs get smaller the interconnects used to communicate within them become the bottleneck of the process, both from a power and a performance perspective [2]. The findings in [2] show that on average the local (intrablock) interconnects contribute 30% to the delay on the worst internal paths of synthesized blocks. They provide a significant contribution to the increase in cell delays, and the interconnects along with repeaters contribute to 31% of the dynamic power. To mitigate these effects, different methods of routing have been suggested to mitigate these effects however these methods tend to increase complexity and don't solve the capacitance or power efficiency issues. The existing literature shows that wired interconnects have a limiting effect on the performance of smaller more compact ICs.

The use of Antenna on Chip (AoC) wireless millimeter-wave (mm-wave) interconnects have been studied as an alternative to wired interconnects. These wireless interconnects use short-range antennas operating in the V frequency band (50-70GHz), also

known as the 60GHz band as that is the center frequency. The use of wireless communication introduces flexibility to the circuit design and reduces power consumption and production costs, as the antennas can be integrated into a standard CMOS process [3]. Another benefit from the use of wireless interconnects is that by operating in the mm-wave frequency range the communication links allow for a high data rate over 1Gb/s for short range of transmission.

1.2 Challenges with Wireless Communications

Wireless interconnects are a promising and emerging innovation for integrated circuit interconnects. With all their promising benefits there are some considerable drawbacks. The antennas are placed within the CMOS stackup in the top silicon dioxide layer above a silicon substrate. The signals from the antenna must propagate through silicon which has a very high relative permittivity of 11.9. The high permittivity and a low resistivity of silicon introduce radiation losses. These losses distort the radiating signal, reduce the signal gain and the antenna efficiency. In addition, there is an increasing demand for wireless links with bit rates over 1Gb/s. Existing on-chip antennas have been generally designed below the 10-GHz frequency spectrum [4].

1.3 Motivation

The motivation for this work is to improve the data communication within and between IC chips by enhancing the signal gain of on-chip antennas using a Frequency Selective Surface (FSS). Specifically, by improving the gain of a directional Yagi antenna

placed in the silicon dioxide of a CMOS stackup. To achieve this a FSS was placed between the antenna and the lossy silicon. An Artificial Magnetic Conductor (AMC) was the FSS chosen and is comprised of a series of periodic metal structures that have a high surface impedance. The AMC's surface produces a reflection coefficient of +1 at its resonant frequency. The AMC layer will be placed below the radiating antenna and act as a barrier that causes the reflected waves to combine constructively with the incident waves at a designed frequency. This was accomplished by selecting and designing the correct AMC geometry to produce a 0˚ phase shift at the plane of incidence. The AMC boundary was chosen because unlike a ground plane it allows for the radiating antenna to be placed much closer than $\lambda/4$ from the reflecting boundary and still produce a 0˚ phase shift at the antenna. Thus, improving the gain of the antenna and the radiation efficiency by shielding the signal from the lossy silicon substrate.

1.4 Major Contribution

As discussed in previous sections there is a large demand for short-range high frequency data transmission between IC chips. In order to achieve this, the 3D modeling software HFSS from ANSYS Electronics Desktop was used to generate simulations. A directive end-fire Yagi-Uda antenna was designed in the $Si0_2$ layer of a CMOS substrate. To enhance the performance of this on-chip antenna, a Jerusalem Cross AMC unit cell was designed using the same CMOS stackup. Then the geometries were tuned to produce 0˚ reflected phase at 60GHz. Once designed, the unit cell was placed under the antenna in a periodic grid to create an AMC layer. The antenna was first tested in a small substrate just large enough to fit the antenna. The model was simulated in three configurations: without

any AMC layer (No AMC), with the AMC layer placed below the feed system (Partial AMC), and with the AMC layer below the entire antenna (Full AMC).

Next the antenna was placed in a 10mm by 10mm CMOS chip. The antenna was tested in the center of the chip, at the front edge of the chip facing out and at the back edge of the chip facing in. The partial and full AMC layers were placed below the antenna in each of these configurations and the impact on the radiation and antenna efficiency was studied. Lastly, the viability of inter-chip transmission was tested by placing simulating the communication between two chips with three different antenna orientations. The first was with the antennas in both chips at the front edge, the second had both antennas in the center of their respective chips, and the third had one antenna at the front edge of the chip and the other antenna in the center of the other chip. These were all simulated with and without the AMC configurations and performance characteristics were compared. Those characteristics being the radiation patterns, directive gain [dB], antenna efficiency, S_{11} [dB] and S_{21} [dB].

1.5 Organization

The work presented in this thesis is organized into five sections. That are briefly described below.

Design of Directional Yagi Antenna: This section discussed the Yagi antenna design from [5] then improved the performance of the antenna by adjusting the beam to end-fire. The Yagi antenna was then designed and optimized in a standard CMOS substrate operating at 60GHz.

Artificial Magnetic Conductors: This section covers the theory behind a frequency selective surfaces (FSS) and specifically an artificial magnetic conductor (AMC). The theory behind a Jerusalem Cross AMC is examined and used for tuning the AMC dimensions. The final AMC unit cell is also designed and simulated in HFSS.

Yagi Antenna in Small CMOS Substrate: This section tests the AMC theory in a small substrate by placing AMC layers below the previously designed Yagi antenna and examining the antenna parameter performance.

Effects of Yagi Antenna Placement Within the Chip: This section explores the effects of antenna placement in a 10mm by 10mm chip on the antenna performance. The antenna was placed in the center of the chip and at the front edge of the chip. In both configurations a partial AMC layer and full AMC layer were placed below the antenna and the performance of each design was examined.

Inter-Chip Transmission: This section looks at the transmission between chips with the antennas placed in different locations in the two chips. First the antennas were placed at the edge of their respective chips facing towards each other. Then the antennas were placed in the center of their respective chips. In the third configuration the first chip had an antenna placed in the center of the chip and the second chip had an antenna placed at the front edge facing the first chip. In all these configurations the results were analyzed without an AMC layer, with a partial AMC layer and with a full AMC layer.

2 Design of Directional Yagi Antenna

2.1 Previous Antenna Design

The Yagi antenna design from [5] was used as a starting point for the antenna design. The conference paper, [5], focuses on the effects that an Artificial Magnetic Conductor (AMC) has on the gain of the antenna when placed below the feed system. They show through simulation that after placing the AMC below the feed system of their antenna their simulated gain was -0.2dBi, measured at 60GHz. This was compared to similar models that did not have the AMC whose gain was -3.5dBi, measured at 60GHz. This was the appeal of [5] for the initial antenna design. For the purposes of this section, only the Yagi antenna will be discussed, the AMC structure will be discussed in a later section. Another appealing aspect of the Yagi antenna presented in [5] was that the antenna was placed in a CMOS substrate for 60GHz transmission. The cross-section view of the CMOS stackup given in the paper is presented in Figure 2-1.

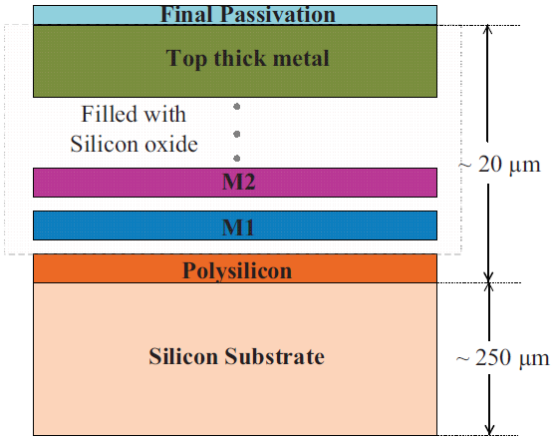

Figure 2-1: Cross-section view of standard CMOS process with multi-layered structure [5].

From Figure 2-1 M1 and M2 refer to the metal layers containing the AMC and the reflector of the antenna, respectively. The top thick metal layer is where the antenna was placed. Their Yagi antenna, shown in Figure 2-2, was designed for a Ground-Signal-Signal-Ground (G-S-S-G) probe pad configuration. The antenna was fed with a coplanar waveguide (CPW), and was composed of a driven element, two directors and one reflector. The antenna was placed in a small substrate 2.2×1.3 mm^2. Given the size of the substrate the radiated fields are mostly propagating in free space and not in the silicon.

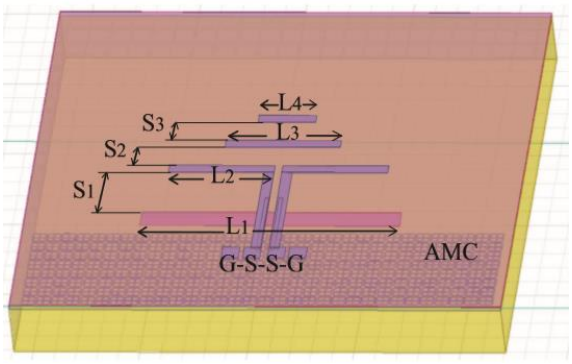

	Dimension	
	In λ_e	In μm
L_1	0.640	1219.84
L_2	0.260	495.56
L_3	0.280	533.68
L_4	0.140	266.84
S_1	0.137	261.12
S_2	0.069	131.51
S_3	0.069	131.51
Pad pitch	-	100

Figure 2-2: Yagi Antenna design and dimensions from [5].

Figure 2-2 shows all the information provided in [5] regarding the antenna dimensions. They left out the dimensions for the CPW length, the spacing between the CPW lines, the size of the G-S-S-G pads, and the placement of the antenna in the substrate. These key dimensions made replicating their design quite difficult. However, the information provided was enough to start with. After replicating their design using HFSS it became clear that there was problem with their design. The problem with their paper is that the main beam generated by the antenna shown in Figure 2-2 is directed at a 40˚ as opposed to a normal end-fire beam, which would be directed straight ahead at 90˚. The 2D and 3D radiation patterns from [5], are shown in Figure 2-3.

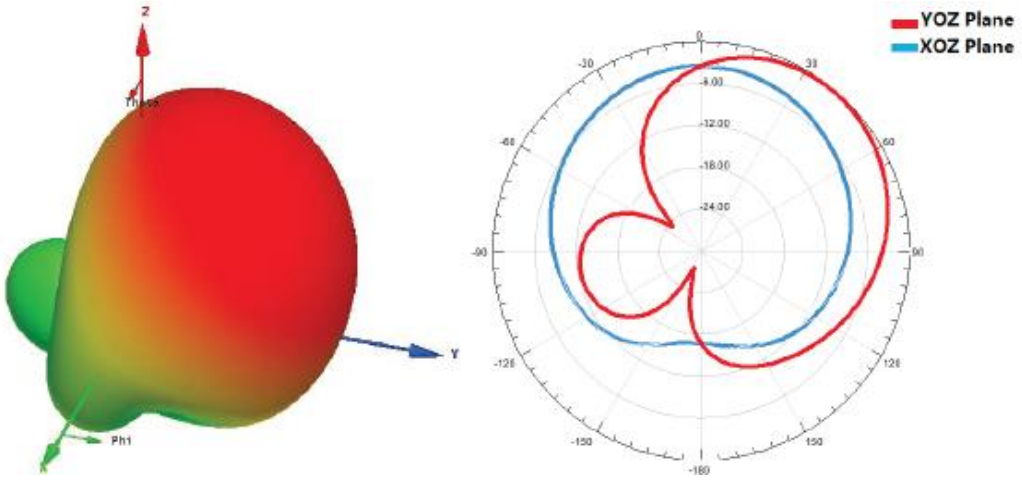

Figure 2-3: 3-D and 2-D gain radiation patterns of Yagi antenna from [5]

The radiation patterns presented in Figure 2-3 show the main beam is directed at about 40˚. The results in this work were replicated in HFSS and resulted in the same skewed beam. Along with these the paper also presented the S_{11} plot which is shown in Figure 2-4.

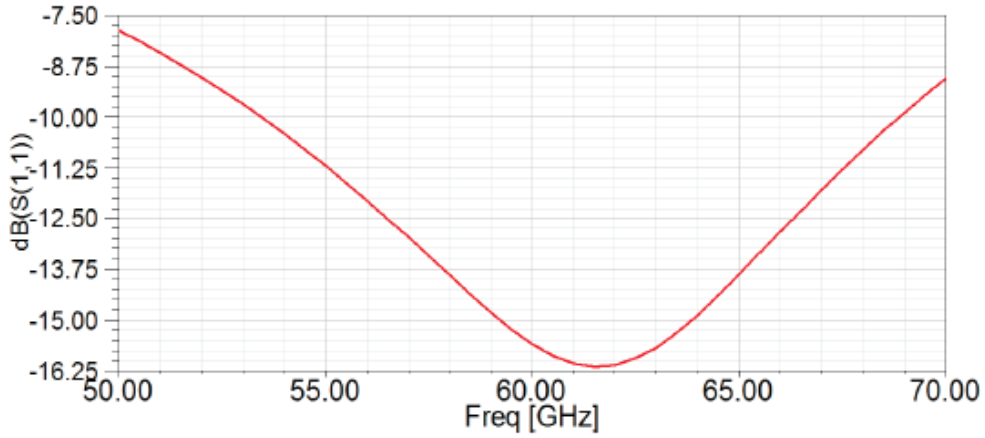

Figure 2-4: Resulting S_{11} [dB] vs. frequency from [5]

Figure 2-4 shows that they achieved about -15.5dB S_{11} at 60GHz. After having understood and replicated the Yagi-antenna from [5] as best as possible, provided that multiple dimensions were missing and had to be surmised. The next step was to tune the antenna to improve the beam steering, such that it is an end-fire beam, and optimize the S_{11} of the antenna.

2.2 Correcting Main Beam to End-Fire

To start with, the stackup used in [5] was changed slightly to meet some manufacturing guidelines. The silicon dioxide (SiO_2) layer was shrunk from 20µm to 7µm all the metal thicknesses were set to 1µm and the silicon substrate is now 275µm thick. The new cross-section view of the substrate and antenna is presented in Figure 2-5.

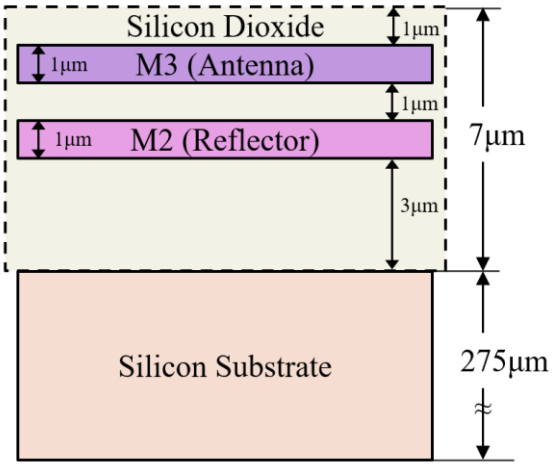

Figure 2-5: Cross-section view of CMOS stackup (with only the antenna)

Next, the Yagi design from [5] was stripped down to a simple dipole antenna with a reflector on metal layer M2 below it. This new dipole was then tuned to direct the main beam at 90˚ straight ahead. The feed system from [5] was changed from a G-S-S-G to a Ground-Signal-Ground (G-S-G) probe configuration to match the hardware available and help fix the beam steering issue. From these probe pads extend the coplanar waveguide (CPW) which feeds the two driven elements of the antenna. The reason the main beam was not at 90˚ was because of imbalances in the feed system of the antenna, which is comprised of the G-S-G pads and the CPW. To steer the beam to 90˚ the spacing between the CPW (S_{cpw}) was tuned and the G-S-G pads were set to the same width as the CPW lines.

Decreasing the CPW spacing caused the main beam of the antenna to rotate clockwise, or in other words the beam angle increased from 45˚ towards 90˚. The CPW spacing was tuned to 1μm. This spacing and the new feed configuration steered the beam to an end-fire configuration.

2.3 Optimization for Antenna Gain and S_{11}

To improve the S_{11} of the antenna the width of the CPW and the length of the dipole were adjusted. Adjusting the CPW width improved the nulls in the S_{11} plot and adjusting the length of the dipole shifted the S_{11} nulls in frequency. The Ansys Designer circuit simulator was used to best match the CPW width to 50Ω, then from there the width was tuned to improve the S_{11}. The final tuned CPW width is 10μm which produced an S_{11} null of -50.58dB. Next the dipole length was increased to shift the null in frequency to 60GHz. Using HFSS a parametric sweep was run to tune the dipole length L_2 and the reflector length L_{1ref}. The reflector length was changed proportionally to the dipole length. The dipole length L_2 was changed to 516μm and the reflector length L_{1ref} was changed to 1222.92μm.

Once S_{11} was optimized two directors were added to the dipole antenna to make the beam more directive and complete the Yagi. The HFSS model of the antenna with the corresponding dimensions is presented in Figure 2-6.

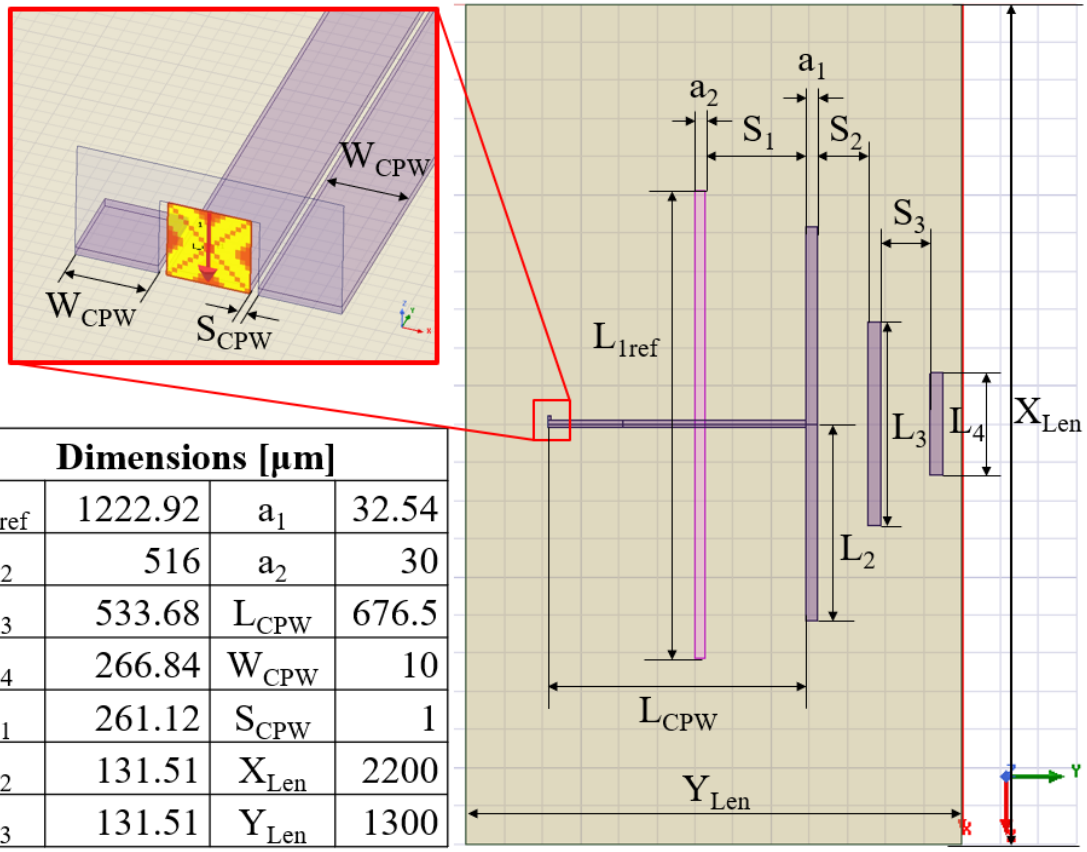

Dimensions [µm]			
L_{1ref}	1222.92	a_1	32.54
L_2	516	a_2	30
L_3	533.68	L_{CPW}	676.5
L_4	266.84	W_{CPW}	10
S_1	261.12	S_{CPW}	1
S_2	131.51	X_{Len}	2200
S_3	131.51	Y_{Len}	1300

Figure 2-6: Model and Dimensions of Optimized Yagi Antenna.

The optimized dimensions of the tuned Yagi antenna are presented in Figure 2-6. The red box in the figure shows how the probe pads were excited in HFSS. The G-S-G pads were excited using a metal bridge to connect the two ground pads and a waveport extending down to the Source pad. The S_{11} plot of the optimized antenna is presented in Figure 2-7 and the radiation pattern of the antenna is presented in Figure 2-8.

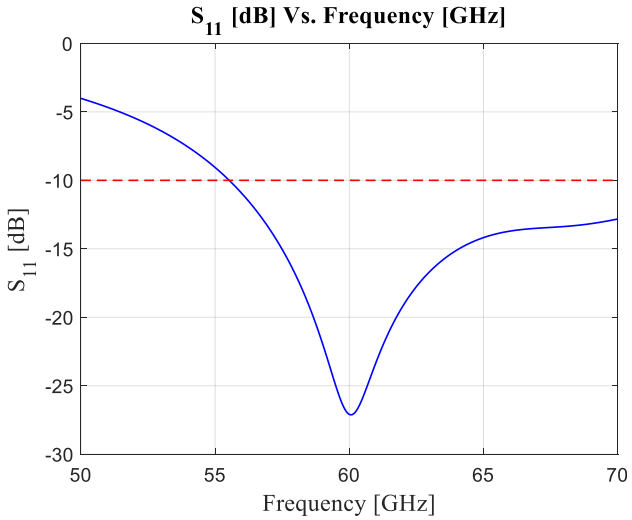

Figure 2-7: S_{11} vs. Frequency plot of optimized Yagi Antenna

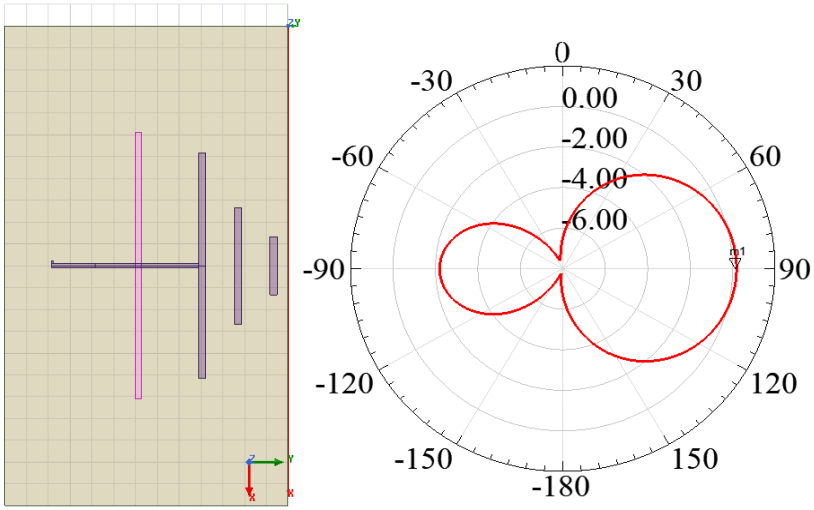

Figure 2-8: Radiation Pattern of Optimized Yagi Antenna

The S_{11} of the optimized antenna is -27.09dB at 60GHz and there is a 10-dB bandwidth from 55.45GHz to beyond 70GHz or 73% of the V-band. The directive gain of the optimized antenna is 0.187 dB, the radiation efficiency is 50% and the front to back ratio is 2.67 dB. Once the antenna was designed and optimized in the small substrate an artificial magnetic conductor can be used to improve its performance, for when it is placed in a larger substrate.

3 Artificial Magnetic Conductors

3.1 Artificial Magnetic Conductor Theory

An Artificial Magnetic Conductor (AMC) is a metal layer similar to a ground plane that is composed of periodic metal structures or unit cells. The unit cell of an AMC structure can be any geometric shape, previous work has explored different geometric configurations such as rectangular patches, snowflake patterns, 'I' shapes, crosses etc.... some of these designs are shown in Figure 3-1.

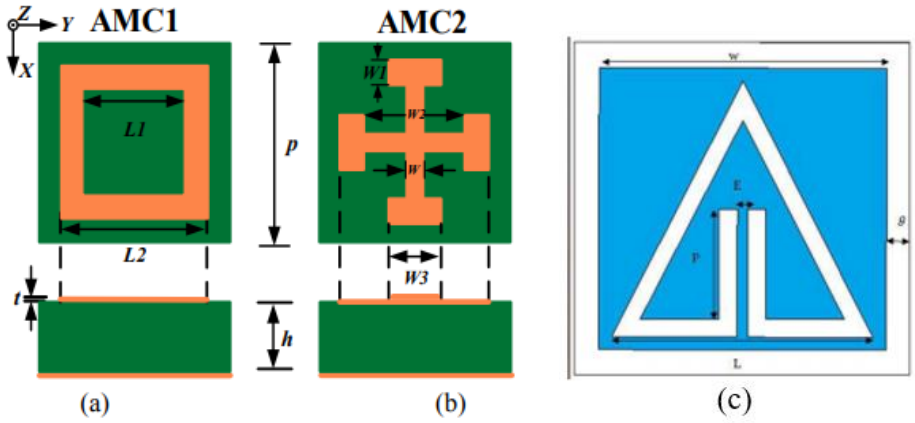

Figure 3-1: AMC unit Cell Designs. Square Loop (a), Jerusalem Cross [6] (b), Triangular Slot [7] (c).

Each design has a different set of critical dimensions that can be tuned to achieve 0˚ phase reflection at a specified resonant frequency. Each unit cell design has a different equivalent circuit model. These circuit models describe the capacitive and inductive elements of the unit cell. These elements correspond to critical dimensions in the unit cell design. By tuning the length and width of these critical dimensions the surface impedance of the cell can be

adjusted. More importantly, from the surface impedance the reflection coefficient and reflected phase can be computed.

To better understand an AMC, it is good to start by understanding the effects of a good conductor or perfect electric conductor (PEC) on the radiation of an antenna. When a PEC or ground plane is placed below a radiating antenna there is a 180˚ or π phase shift at the ground plane. If the PEC is placed a quarter wavelength below the antenna, then the wave will hit the PEC with a phase of π/2 then be shifted by π from the PEC and travel another π/2 to reach the antenna again. The resulting phase is 2π or 0˚, so in this case the reflected wave would combine constructively with the incident wave. This is illustrated in Figure 3-2 where *wave 1* is the incident wave and *wave 2* is the reflected wave.

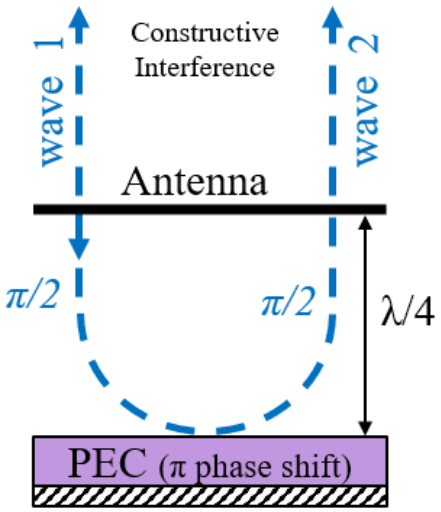

Figure 3-2: Antenna placed λ/4 from PEC

However, this requires that the antenna is placed a minimum of λ/4 from the PEC to have constructive interference. If the antenna is placed any closer to the PEC than λ/4 there is a phase shift so the incident and reflected waves will combine destructively [8], thus reducing the radiation of the antenna. This is illustrated in Figure 3-3.

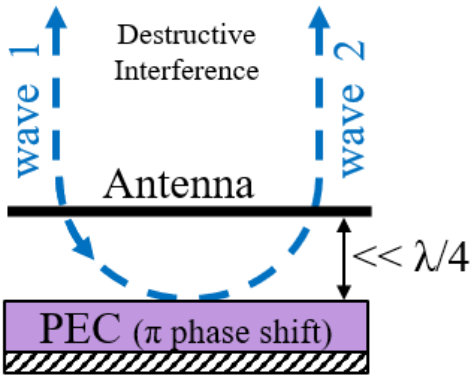

Figure 3-3: Antenna placed much closer than λ/4 to PEC

An Artificial Magnetic Conductor (AMC) is a frequency selective surface (FSS) that acts as a perfect magnetic conductor (PMC) instead of a PEC. A PEC has a reflection coefficient -1 while a PMC has a reflection coefficient of +1 of Unlike the PEC a PMC has no phase shift at the surface of the conductor because magnetic conductors support surface waves. An AMC acts like a PMC at a specific frequency, which is what makes it frequency selective. This allows for the AMC plane to be placed much closer than λ/4 to the radiating antenna. At the resonant frequency of the AMC the reflected waves and the incident waves combine constructively because they are in phase at the plane of the antenna, thus enhancing the radiated field. This is illustrated in Figure 3-4.

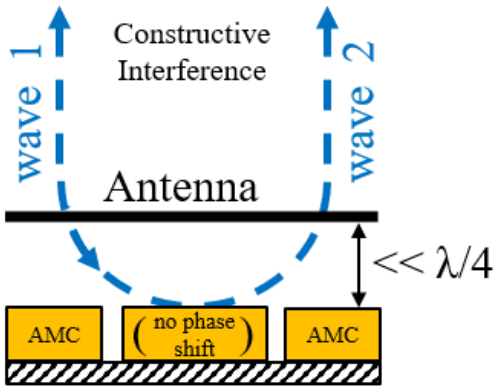

Figure 3-4: Antenna placed much closer than λ/4 to an AMC

3.2 Jerusalem Cross AMC Theory

Now that the practical operation of an AMC plane is understood the theory behind the actual structure can be analyzed. An AMC is also known as a High Impedance Surface (HIS) because at a specific frequency the surface impedance of the AMC approaches infinity. At this frequency the reflected phase approaches zero [9]. This is what allows the incident and reflected waves to combine in phase, thus increasing the radiation efficiency and gain of the antenna. For this work a Jerusalem Cross AMC (JC-AMC) was the chosen unit cell design. The operating frequency of the Yagi antenna is 60 GHz, so the AMC unit cell was designed for this resonant frequency. The equivalent circuit model of a Jerusalem Cross AMC is presented in Figure 3-5.

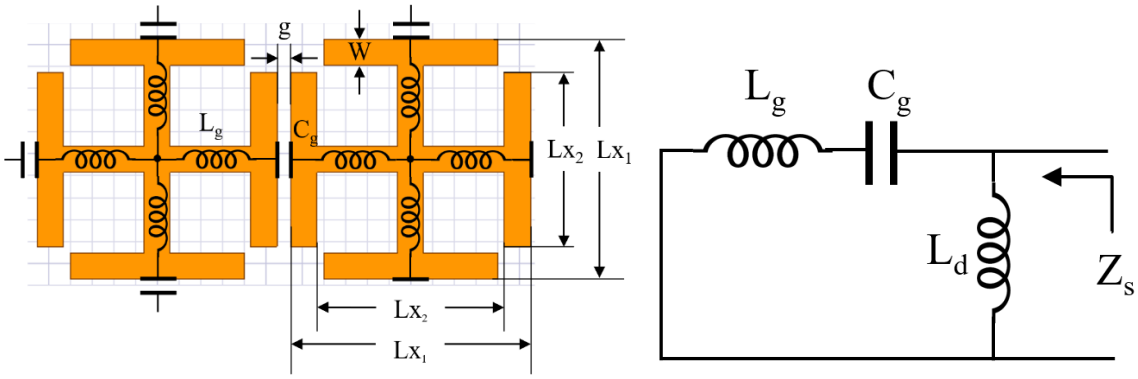

Figure 3-5: JC-AMC Equivalent Circuit Diagrams

From Figure 3-5 the L_d is the dielectric inductance from the , L_g is the grid inductance, C_g is the grid capacitance, and Z_s is the surface impedance. The surface impedance comes from the equivalent circuit diagram in Figure 3-5 and is given by equation (1). This equation comes from [10].

$$Z_s(\omega) = j\omega L_d \frac{1 - \omega^2 L_g C_g}{1 - \omega^2 (L_g + L_d) C_g} \tag{1}$$

Where ω is the angular frequency equal to $2\pi f$. Each of the inductances and capacitances are related to the physical dimensions of the AMC by the equations (2) – (4).

$$L_g = \frac{Z_0}{j\pi f}\tan\left(\frac{k(Lx_1 - W)}{2}\right) \tag{2}$$

$$C_g = \frac{2Lx_2}{\pi}\epsilon_0\epsilon_{reff}\cosh^{-1}\left(\frac{g - 2W}{g}\right) \tag{3}$$

$$L_d = \frac{\eta_0}{\sqrt{\epsilon_r}}\frac{\tan(kh)}{2\pi f} \tag{4}$$

From the equations above, *k* is the wave number, *h* is the height of the silicon substrate, ε_r is referring to the dielectric constant of the substrate, in this case silicon, 11.9, and ε_{reff} is the effective dielectric constant of the CMOS substrate given by standard equations in literature. From the above equations the physical dimensions are related to the capacitive and inductive elements which make up the surface impedance. L_g related to the width *W* and Lx_1, C_g is related to Lx_2, *g* and *W*, and L_d is related to the dielectric substrate height, *h*. The surface impedance, Z_s, is related the reflected phase by the standard expression shown in (5).

$$\phi_{11} = \angle\Gamma = \frac{Z_s - \eta_0}{Z_s + \eta_0} \tag{5}$$

Using MATLAB and equations (1) – (5) a function was created that took four variable inputs: *g*, *W*, Lx_1, and Lx_2. This function outputs the surface impedance Z_s and the reflected phase. By plotting either of these over a large frequency range the AMC dimensions can be tuned for a resonant frequency of 60GHz. For the surface impedance the resonant frequency is where the surface impedance peaks, for the reflected phase the resonance is where there is a 0˚ phase reflection.

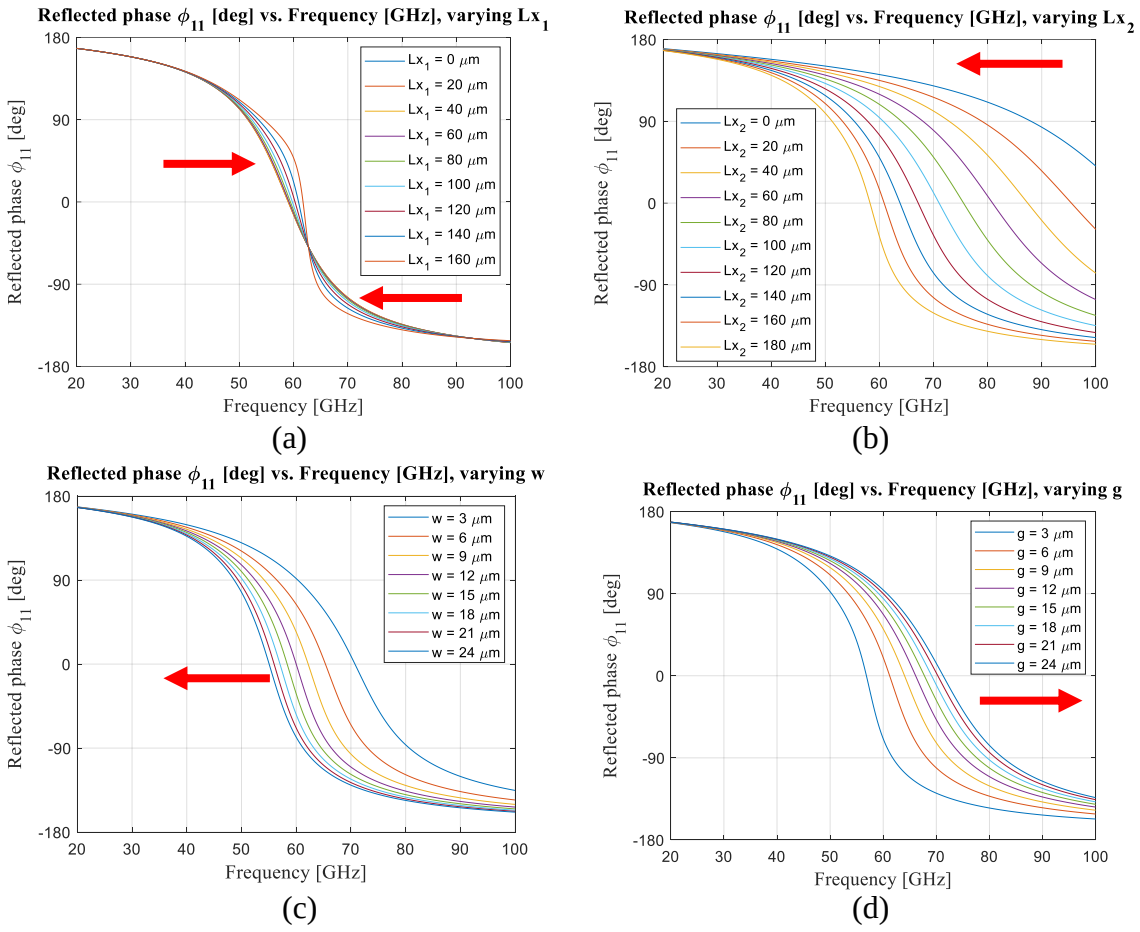

Figure 3-6: MATLAB plots Tuning AMC dimensions: Tuning Lx_1 (a), Tuning Lx_2 (b), Tuning W (c), Tuning g (d).

The plots in Figure 3-6 show MATLAB sweeps of the four critical dimensions of the AMC unit cell. These sweeps show how each individual dimension affects the reflected phase of the AMC. The red arrows in the figure show how the pattern changes as the sweep variable increases. Figure 3-6(a) shows that as Lx_1 increases the positive ϕ_{11} values move up in frequency while the negative values move down, also narrowing the ±90˚ bandwidth. Figure 3-6 (b) and (c) shows that as Lx_2 and W increase ϕ_{11} moves down in frequency. Figure 3-6(d) shows that as g increases ϕ_{11} moves up in frequency. These dimensions were tuned to achieve the ideal 0˚ phase reflection at 60GHz using this MATLAB function based

on the empirical formulas. The resulting theoretical dimensions were Lx_1 = 110 μm, Lx_2 = 166.44 μm, W = 12 μm, and g = 5μm.

3.3 Jerusalem Cross AMC Unit Cell Design

Now that the theory behind the JC-AMC has been examined the AMC unit cell can be simulated and further tuned in HFSS. The AMC unit cell was designed using the EM solver HFSS on the CMOS stackup shown in Figure 3-7.

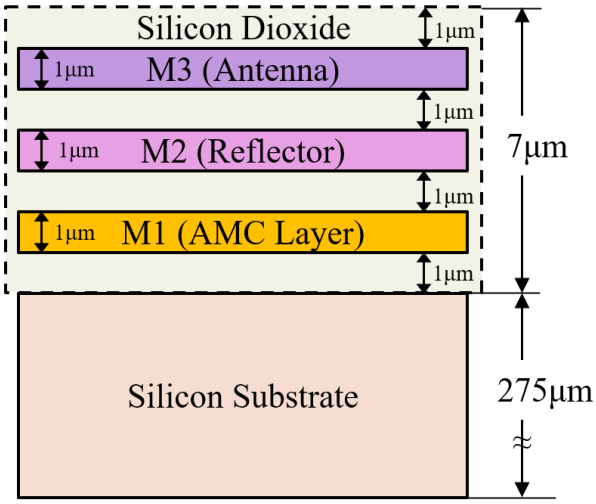

Figure 3-7: Cross-section view of CMOS stackup

The Jerusalem Cross was placed in silicon dioxide on the silicon substrate without the top two metal layers (M2 and M3), as shown in Figure 3-7. In HFSS an air box was created above the silicon dioxide with a waveport at the top. The model consists of two perfect electric conductor (PEC) walls and two perfect magnetic conductor (PMC) walls [5]. These walls are the boundaries that represent neighboring unit cells. Images of the HFSS design are shown in Figure 3-9.

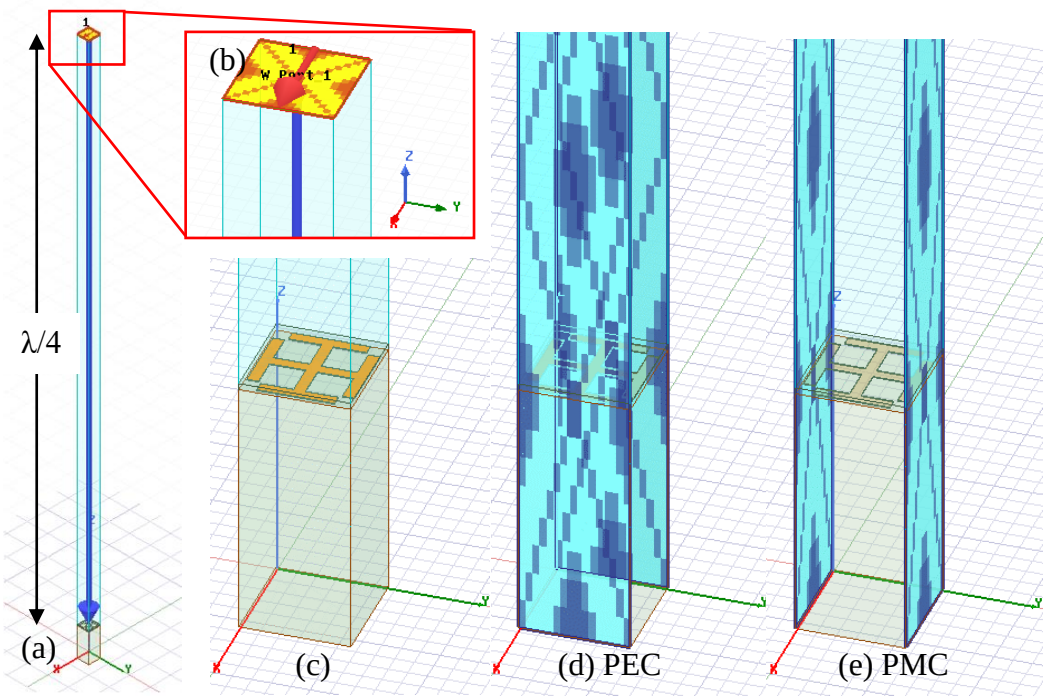

Figure 3-8: AMC unit Cell. HFSS model with de-embedding (a), waveport excitation (b), PEC boundary (d), PMC boundary (e).

As shown in the above figure the simulation was excited from a waveport place λ/4 above the AMC. The integration line on the waveport is directed between the two PEC boundaries and perpendicular to the PMC boundaries. The Jerusalem Cross dimensions were adjusted to shift the reflected phase angle at 60GHz to 0˚. The dimensions of the Jerusalem Cross were designed based originally on the theoretical results from the MATLAB function. The AMC unit cell dimensions are presented in Figure 3-9.

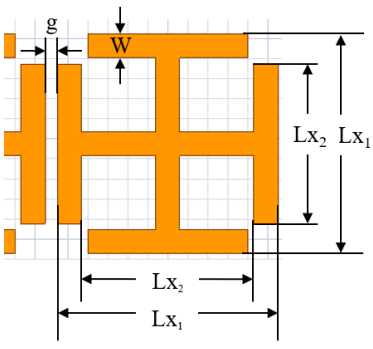

AMC Dimensions	
Lx_1	110 µm
Lx_2	80 µm
W	12 µm
g	5 µm

Figure 3-9: AMC Unit Cell Geometry and Dimensions

The width W and the spacing between the cells, *g*, are the critical dimensions. When simulating in HFSS these dimensions had the largest effect on the phase plot. The spacing between the cells *g* is critical because it determines the capacitance between each cell. In the model the PEC and PMC walls are placed *g*/2 from the edge of the AMC. This spacing was tuned to shift the reflected phase in frequency by adjusting the capacitance. The final dimensions of the AMC unit cell as defined in Figure 3-9 are Lx_1 = 110µm, Lx_2 = 80µm, W = 12µm, and g = 5µm. The only difference between these values and the MATLAB values is Lx_2. The reflected phase measured from the AMC unit cell over frequency is shown in Figure 3-10.

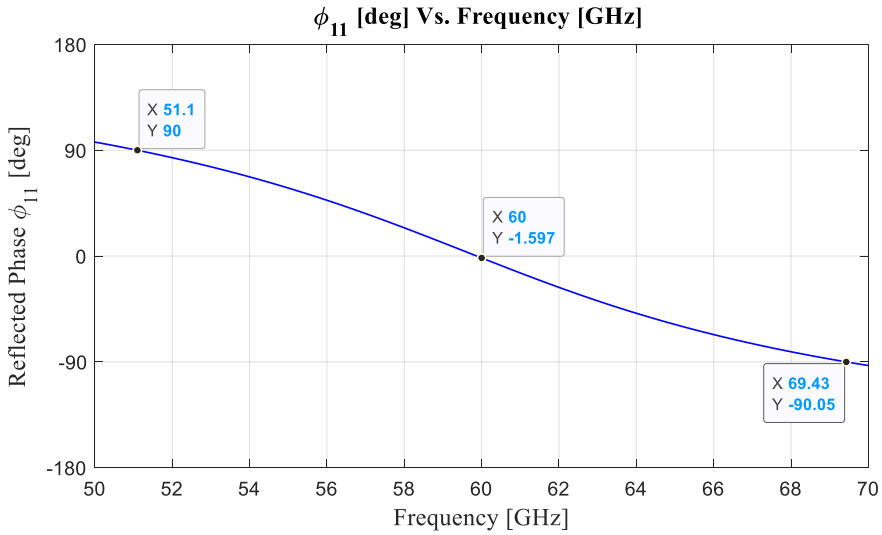

Figure 3-10: AMC Unit Cell S_{11} Phase vs. Frequency

The reflected phase at 60GHz is approximately 0˚ as shown in Figure 3-10. There is a very wide ±90˚ bandwidth from 51.1GHz to 69.43GHz, which is 85.9% of the V-band.

4 Yagi Antenna in Small CMOS Substrate (2.2 × 1.3 mm^2)

The Yagi antenna was optimized in a substrate just large enough to fit the antenna as discussed in section 2. This was to see the radiation pattern of the antenna with limited interference from the silicon, since most of the radiation is in free space. Due to this it also made sense to first examine the effects the AMC has in this small substrate. The Jerusalem Cross AMC unit cells designed in the previous section were placed in a grid below the antenna in three different configurations. In the first configuration a layer of unit cells was arranged under only the feed system of the antenna, this will be referred to as a *Partial AMC*. In the second configuration the AMC unit cells were arranged in a grid below the entire antenna, this will be referred to as the *Full AMC*. The third configuration does not include an AMC layer at all, this will be referred to as *No AMC*. The partial AMC layer was arranged below the CPW from the G-S-G pads to the reflector. The HFSS models of the Yagi antenna in all three configurations are shown in Figure 4-1.

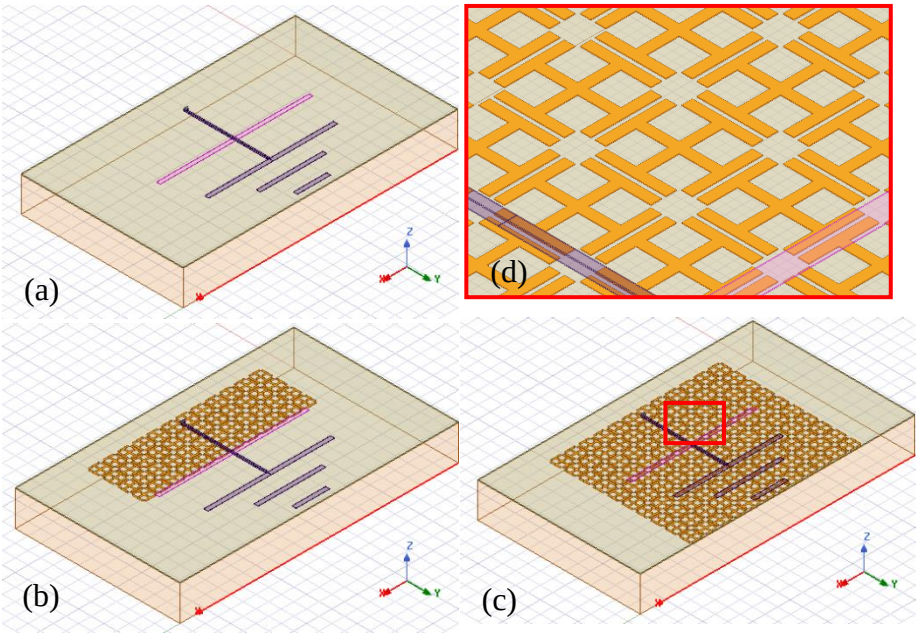

Figure 4-1: HFSS Models of Yagi antenna: No AMC (a), Partial AMC (b), Full AMC (c), Enlarged view of AMC (d).

The S_{11} plot of all three configurations is shown below along with a red dashed line indicating the 10dB level.

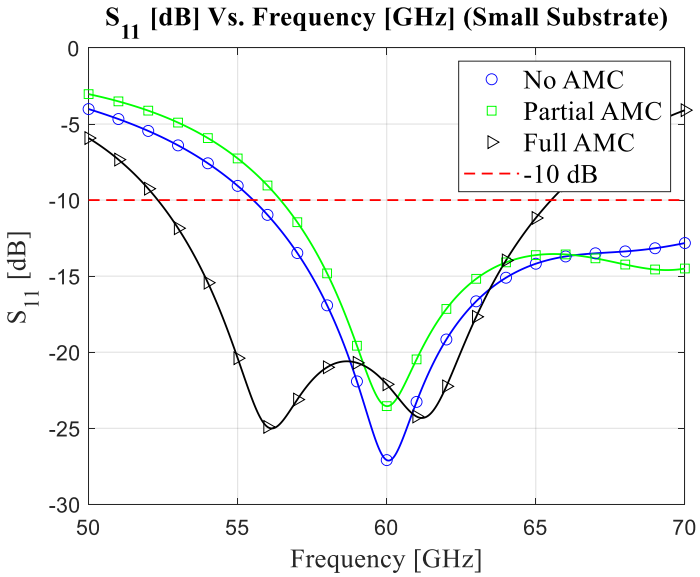

Figure 4-2: S_{11} [dB] vs. frequency plot in small substrate

From Figure 4-2 the S_{11} [dB] for all configurations perform well. The driven element length L_2 was adjusted for each cnofiguration to shift the S_{11} plot in frequency. The reflector length L_{1ref} was adjusted according to the following equation.

$$L_{1ref} = 1.185(2 \cdot L_2) \quad (6)$$

This equation was used to adjust the driven element length for all antenna configurations through out this work. The corresponding S_{11} at 60GHz for the antenna with a partial AMC is -23.54dB and there is a 10-dB bandwidth from 56.37dB to above 70dB which covers 68% of the V-band. The corresponding S_{11} at 60GHz for the antenna with a full AMC is -22.11 dB and there is a 10-dB bandwidth which covers 66% of the V-band. These results are tabulated in Table 4-1.

Table 4-1: Summary of AMC Performance on a Small Substrate

Small Substrate	Driven Element LengthsL_2 [µm]	S_{11} [dB] at 60GHz	10dB Bandwidth
No AMC	516	-27.09	73%
Partial AMC	500	-23.54	68%
Full AMC	425	-22.11	66%

As shown in the table above, the AMC layers slightly decrease the S_{11} [dB] and the 10dB bandwidth. Overall, the S_{11} performance was not significantly affected. The radiation patterns are presented in Figure 4-3.

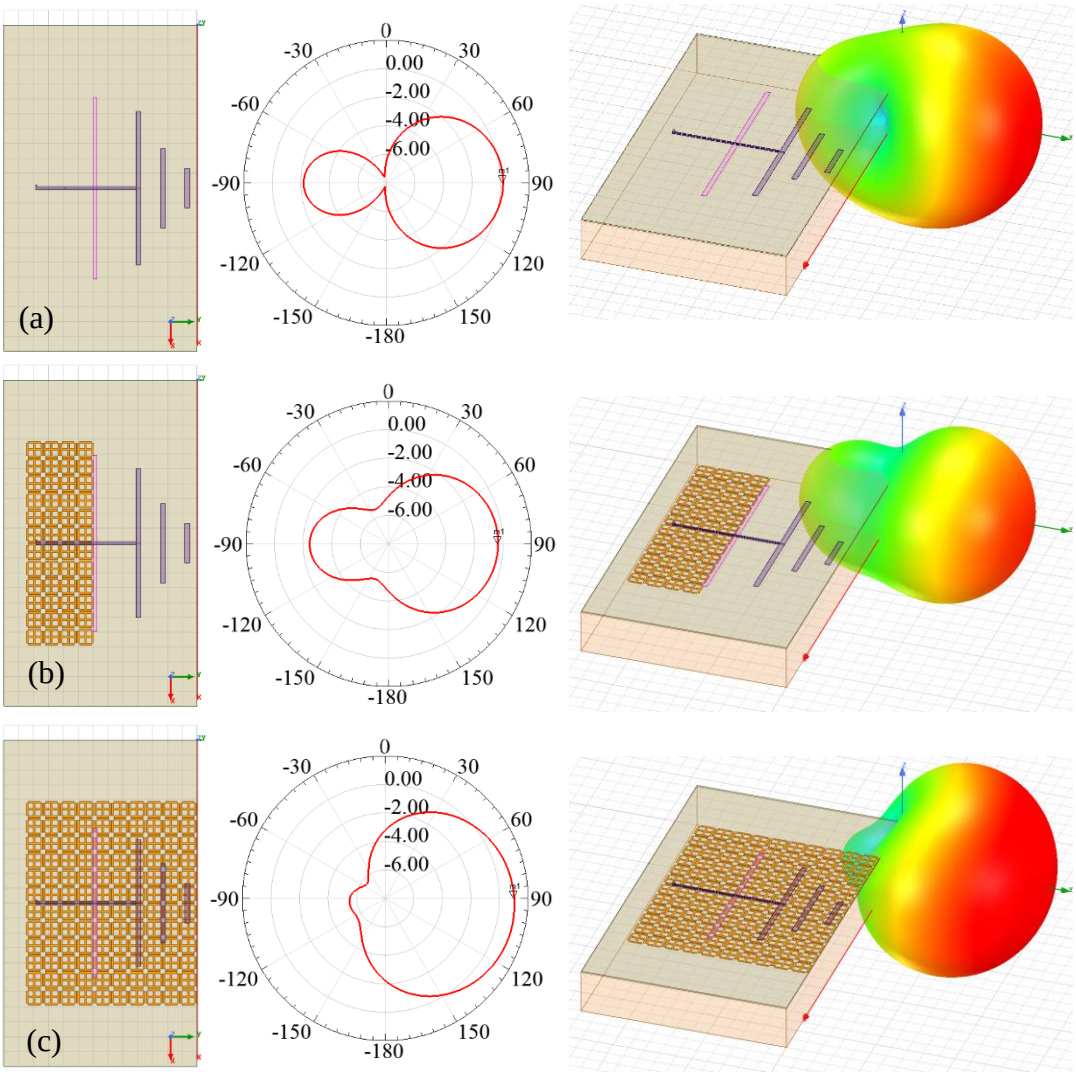

Figure 4-3: Antenna Layout with 2D and 3D Radiation Patterns: No AMC (a), Partial AMC (b), Full AMC (c).

The 2D and 3D radiation patterns in Figure 4-3 show that the large AMC significantly improves the directive gain from 0.187 dB without the AMC to 1.036 dB. The antenna efficiency increased from 50% to 51% and the front to back ratio (F/B) increased from 2.67dB to 6.95dB. On the other hand the partial AMC reduced the directive gain to -0.33 dB. It also decreased efficiency to 44% and the F/B to 2.28dB. Placing the AMC under only the feed line likely enhanced the back lobe and not the front thus reducing the directive gain and increasing the back lobe. These results are presented in Table 4-2. Next these three configurations will be examined in a larger substrate.

Table 4-2: Antenna parameters for small substrate

	No AMC	Partial AMC	Full AMC
Directive Gain [dB]	0.187	-0.33	1.036
Radiation Efficiency	50%	44%	51%
Front to Back Ratio [dB]	2.67	2.28	6.95

5 Effects of Yagi Antenna placement within the Chip

Next the same Yagi antenna designed in the small substrate was optimized in a larger 10mm by 10mm substrate, which will be referred to as the chip. The chip has the same stackup as the AMC unit cell shown in Figure 3-7. The antenna was placed in three different locations on the chip: the center of the chip, the front edge facing out of the chip, and the back edge facing into the chip.

5.1 Yagi Antenna in Different Locations on Chip without AMC

The antenna was placed in the three locations on the chip to see how the antenna's location changes the directive gain and antenna efficiency. The expectation is that placing the antenna on the back edge facing in will have the worst performance and placing the antenna on the front edge facing out will have the best. This hypothesis assumes that waves propagating through more silicon will perform worse. Images of the three HFSS models showing the different arrangements are presented in Figure 5-1.

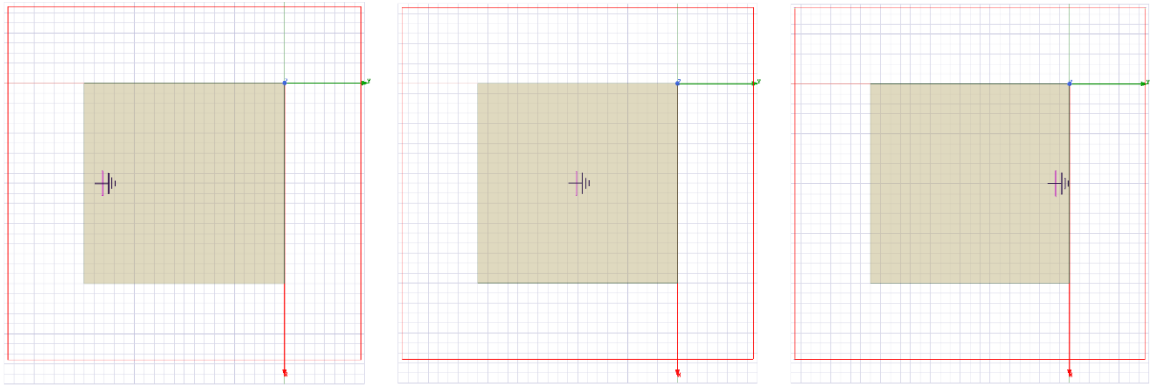

(a) (b) (c)

Figure 5-1: Images of different antenna arrangements without AMC: Back Edge (a), Center (b), Front Edge (c).

In Figure 5-1 The center square, is the 10mm by 10mm CMOS substrate. The red outer box is the boundary of the radiation box used in HFSS. In Figure 5-1 (a) the antenna is placed at the far-left edge of the substrate with the front of the antenna 1.55mm from the left edge. In Figure 5-1(b) the center of the antenna is centered on the substrate and in Figure 5-1(c) the front of the antenna is 50µm from the right side of the substrate. The length of the driven elements and the reflector were adjusted for each arrangement to shift the S_{11} null in frequency to 60GHz. The S_{11} plots of these three configurations are presented in Figure 5-2.

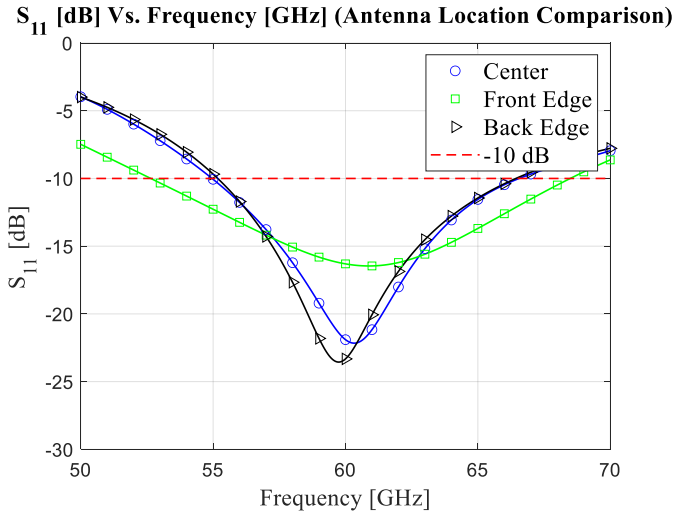

Figure 5-2: S_{11} [dB] vs. Frequency for different antenna locations without AMC.

From Figure 5-2 the Center and back antenna placements have relatively similar performance while the S_{11} of the front edge placement is not as deep but spans a wider 10dB bandwidth. However, all three performed relatively well. The electric field patterns were plotted for each arrangement and are shown in Figure 5-3.

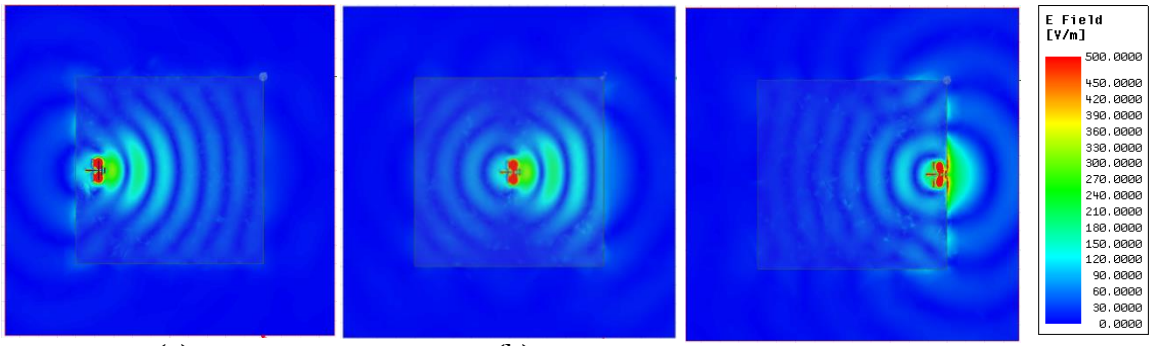

(a) (b) (c)

Figure 5-3: E-Field patterns for different antenna placements without AMC: Back Edge (a), Center (b), Front Edge(c).

The three simulations shown in Figure 5-3 are all without an AMC layer. Figure 5-3(a) shows the E-field pattern propagating into the substrate but fading near the other side of the chip. Figure 5-3(b) shows a fair amount of back radiation and Figure 5-3(c) shows a lot of radiation into free space as well as back radiation into the chip. The 2D radiation patterns for these arrangements are shown in Figure 5-4. The radiation patterns are from the plane of the chip, or the Azimuth plane. They are also displayed in the same orientation as the antennas in Figure 5-1 and Figure 5-3.

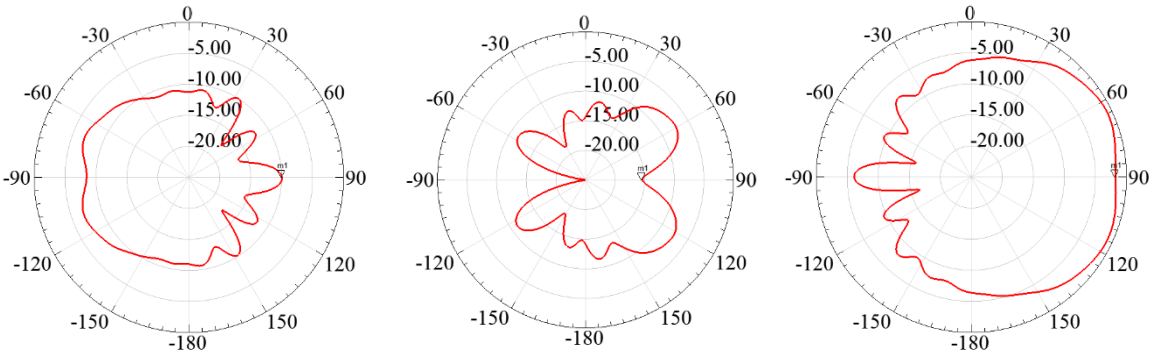

(a) (b) (c)

Figure 5-4: Radiation patterns in for different antenna locations [dB]: Back Edge (a), Center (b), Front Edge (c).

The three radiation patterns presented in Figure 5-4 behave as expected. The radiation pattern of the antenna on the back edge is mainly directed into free space away from the

substrate, which is the opposite direction of the antenna. The radiation pattern for the antenna in the center of the substrate is distorted with nulls at ±90˚ and the radiation pattern for the antenna at the front edge pointing into free space shows the best gain directed out of the chip. The directive gains at 90˚ from Figure 5-4 (a), (b), and (c) are -9.94 dB, -15.37 dB, and -1.72 dB respectively. These results and the antenna efficiencies are presented in Table 5-1 along with the S_{11} performance.

Table 5-1: Antenna Parameters for Different Antenna Locations

	Back Edge	Center	Front Edge
Directive Gain [dB]	-9.94	-15.37	-1.72
Radiation Efficiency	8.1%	10.5%	39.1%
Driven Element Lengths (L2) [μm]	500	512	545
S_{11} [dB] at 60GHz	-23.32	-21.90	-16.32

The radiation efficiency of the antenna at the front edge is by far the best and the efficiency of the antenna at the back is the worst. That makes sense because the input power in the front antenna is mostly directed into free space, while the power radiating from the antenna on the back edge is getting directed back at the feed and into free space as opposed to into the lossy substrate. The antenna in the center has marginally better efficiency than that on the back edge, likely because most of the power is lost from interference with the silicon substrate. Out of these three orientations the antenna at the front edge appears to be the leading contender for inter-chip transmission. While the antennas at the back edge and center of the chip may be more beneficial for intra-chip transmission, if they were enhanced. Next the AMC layer presented in the previous section, with the smaller substrate, was introduced into the center and front edge arrangements, to improve their gain and radiation efficiency.

5.2 Yagi Antenna placed in the Center of the Chip with AMC

The 10×10 mm^2 substrate with the Yagi antenna in the center was examined first using the AMC configurations discussed in section 4. To minimize the effects of the silicon substrate on the Yagi antenna an AMC layer was placed below the antenna. All three AMC configurations were explored: without the AMC, with the partial AMC, and with the full AMC. In this case the term *Full AMC* still refers to a grid of AMC unit cells just large enough to cover the area directly below the antenna. The same sized grid as discussed in section 4. The HFSS models of the partial and full AMC are presented in Figure 5-5.

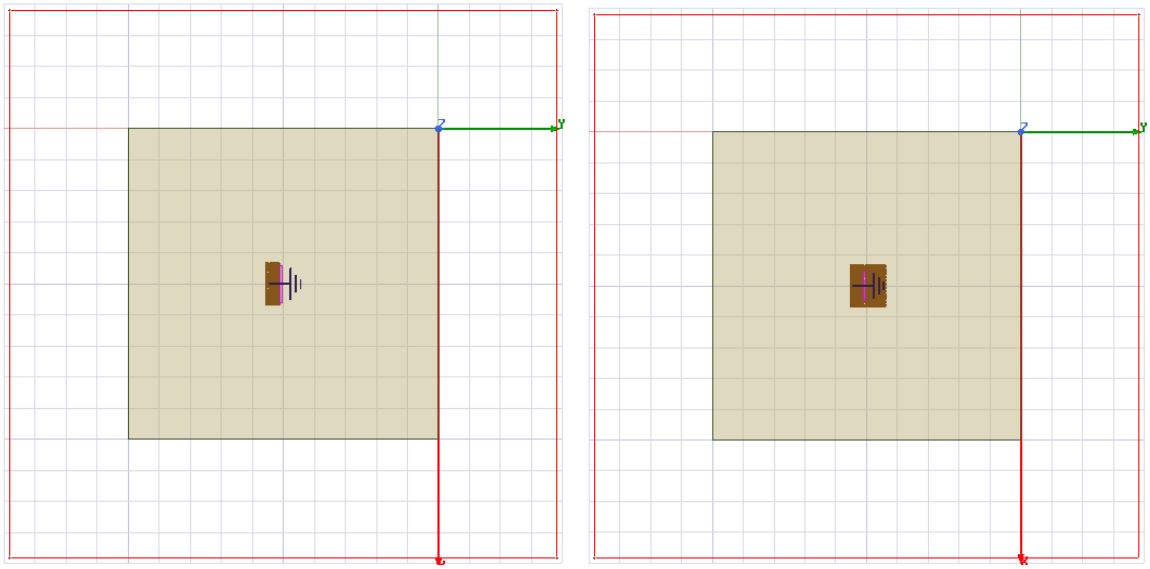

(a) (b)

Figure 5-5: Antenna in the Center of Chip. Partial AMC (a), Full AMC (b).

The AMC layer was not extended to the entire 10mm by 10 mm chip due to limitations in the available computing cluster. A larger array of AMC unit cells requires more RAM then was available to complete the simulation. The S_{11} of these three configurations is presented in Figure 5-6.

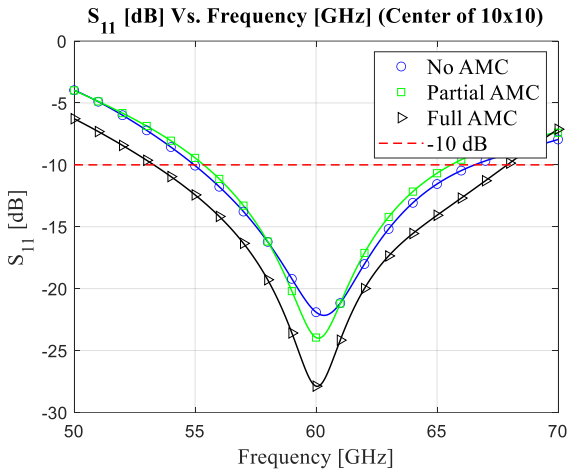

Figure 5-6: S_{11} [dB] vs. Frequency for Antenna in the center of the Chip

The director lengths were adjusted to improve the S_{11}. From the above figure the S_{11} of the antenna with the partial AMC is -23.95 dB at 60GHz and there is a 10-dB bandwidth of 51.2%. The S_{11} of the antenna with the full AMC is -27.88 dB at 60GHz and there is a 10-dB bandwidth of 73.05%. Adding the AMC layers has improved the S_{11} plot in both configurations. The results described above are all collected in Table 5-2 at the end of this section. The plots of the E-field magnitude for the three different configurations are shown in Figure 5-7.

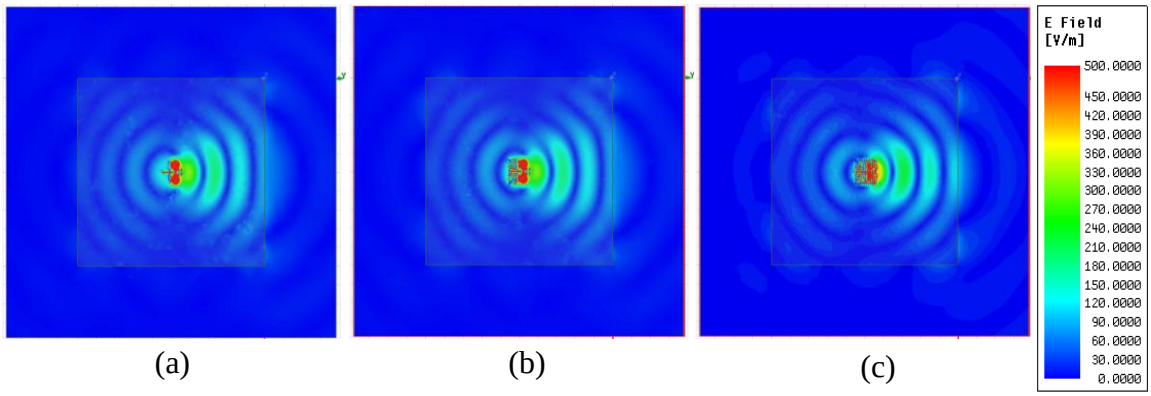

(a) (b) (c)

Figure 5-7: E-Field Patterns of antenna in n the center of the chip: No AMC (a), Partial AMC (b), Full AMC (c).

As shown in Figure 5-7 the full AMC increases the E field in front of the antenna and decreases the pattern behind it. While on the other hand the partial AMC seems to increase

the radiation behind the antenna and the forward pattern seems the same. These assessments are better understood from the radiation patterns, which are shown in Figure 5-8.

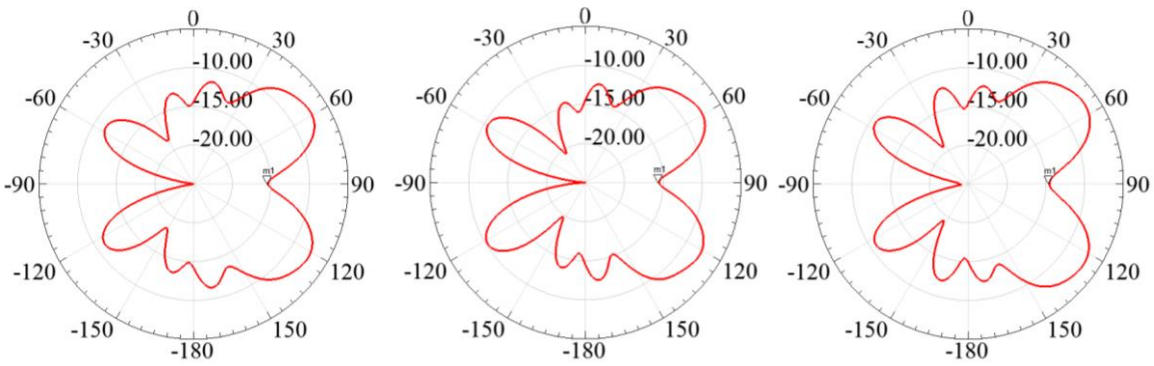

(a) (b) (c)

Figure 5-8: 2D Radiation patterns of antenna in the Center [dB]: No AMC (a), Partial AMC (b), Full AMC (c).

In Figure 5-8(c) the directive gain has increased from -15.37 dB without an AMC to -14.55 dB with the full AMC and the antenna efficiency increased from 10.4% to 10.8%. The directive gain of the antenna with the partial AMC got marginally worse it went down to -15.54dB and the efficiency declined to 9.44%. These results mirror those of the antenna on the smaller substrate. The partial AMC is likely enhancing only the feed system and not the directed portion, which is enhancing the radiation behind the antenna. While on the other hand the full AMC is improving the overall radiation and shielding the antenna from the lossy silicon. These results are presented in Table 5-2.

Table 5-2:AMC Performance of an antenna in the center of a 10×10mm Substrate with AMC

	Director Length L_2	S_{11} [dB] at 60GHz	Directive Gain [dB]	Radiation Efficiency	10dB Bandwidth
No AMC Layer	512 µm	-21.90	-15.37	10.45%	58%
Partial AMC Layer	507 µm	-23.95	-15.54	9.44%	51.2%
Full AMC	410 µm	-27.88	-14.55	10.78%	73.05%

5.3 Yagi antenna placed at the Front Edge of the chip with AMC

Next the Yagi antenna was placed at the edge of the 10×10 mm^2 chip. This was done to examine the viability of inter-chip transmission. The full AMC layer was added below the Yagi antenna. The HFSS models of the partial and full AMC are presented in Figure 5-9 and the S_{11} of these three configurations is presented in Figure 5-10.

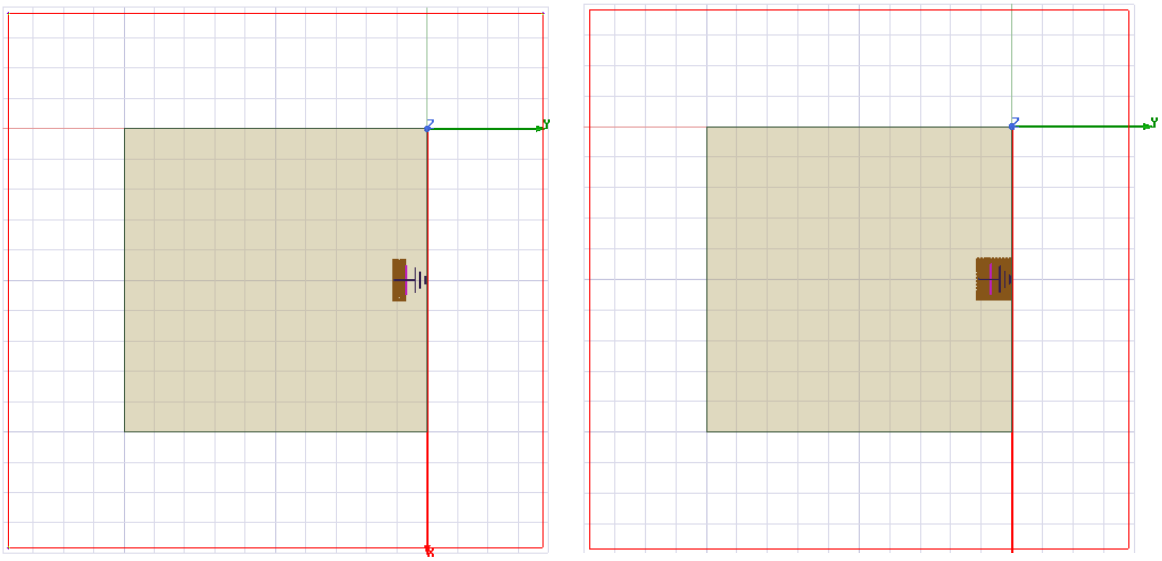

(a) (b)

Figure 5-9: Antenna at the front edge with AMC: Partial AMC (a), Full AMC (b).

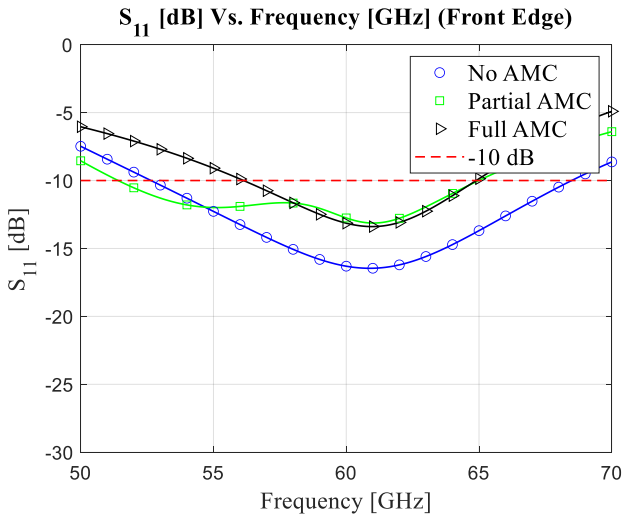

Figure 5-10: S_{11} [dB] vs. Frequency for Antenna at the front edge of the Chip

The director lengths were adjusted to improve the S_{11} for the different configurations as in the previous arrangements. From the above figure the S_{11} of the antenna with the partial AMC is -13.12 dB at 60GHz and there is a 10-dB bandwidth of 66.7%. The S_{11} of the antenna with the full AMC is -27.88 dB at 60GHz and there is a 10-dB bandwidth of 73.05%. Adding the AMC layers has improved the S_{11} plot in both configurations. The plots of the E-field magnitude for the three different configurations are shown in Figure 5-11and the radiation patterns are shown in Figure 5-12.

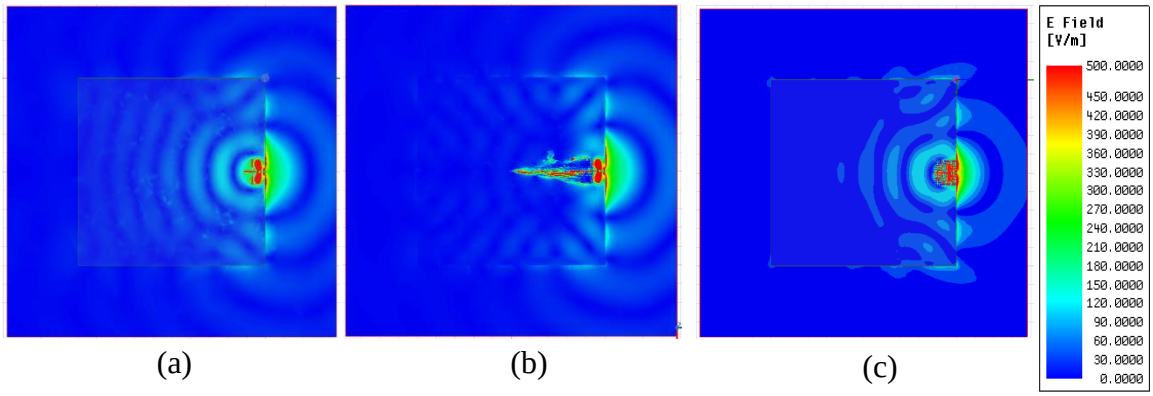

(a) (b) (c)

Figure 5-11: E-Field Patterns: No AMC (a), Partial AMC (b), Full AMC (c).

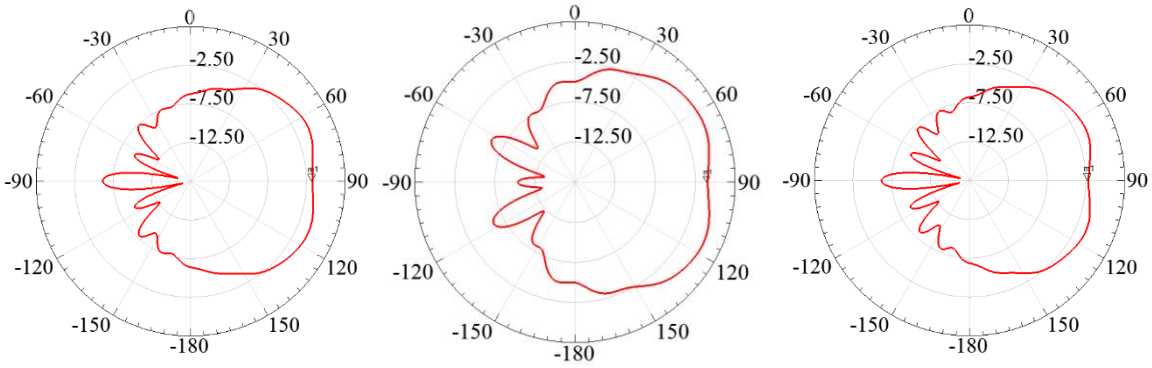

(a) (b) (c)

Figure 5-12: 2D Radiation patterns in dB: No AMC (a), Partial AMC (b), Full AMC (c)

As shown in Figure 5-11 the full AMC layer increases the Electric field in front of the antenna as well as a bit behind it. The Electric field pattern for the antenna with the partial

AMC, Figure 5-11(b), shows thin lines of high electric field density extending from the feed lines to the center of the substrate. This is due to the meshing in HFSS, likely because of small geometries and boundary conditions inherent in the AMC design. The meshing issue should not have a significant impact on the results obtained in the simulation. The radiation patterns for these configurations are shown in Figure 5-12. In Figure 5-12(a) and (b) show the radiation patterns for the antenna without the AMC and with the Partial AMC respectively. After adding the partial AMC, the gain increased from -1.72 dB to -0.93 dB with the partial AMC, which is a 46% increase in the directive gain. The radiation efficiency increased from 39% to 46%. While the directive gain of the full AMC has decreased to -2.15 dB and the antenna efficiency decreased to 35.43%. From these results it is clear that the partial AMC is more beneficial to the antenna's performance when the antenna is placed at the edge of the substrate. The results described above are all collected in Table 5-3.

Table 5-3:AMC Performance Summary of an antenna at the edge of a 10×10 Substrate

	Director Length L_2	S_{11} [dB] at 60GHz	Directive Gain [dB]	Radiation Efficiency	10dB Bandwidth
No AMC	545 μm	-16.31	-1.72	39.05%	78.95%
Partial AMC	530 μm	-13.12	-0.93	46.28%	66.7%
Full AMC	425 μm	-13.14	-2.15	35.43%	44.25%

6 Inter-Chip Transmission

This next section explores the communication between two chips with the Yagi antennas placed at different locations within the chips facing each other. The same 10mm by 10mm chips examined in sections 5.2 and 5.3 were placed on 1.575mm thick FR4 substrate and separated by 10mm. The FR4 substrate has a dielectric permittivity of 4.4 and a loss tangent of 0.02. Three antenna configurations were examined: both chips with antennas at the front edge of their respective chips, both chips with antennas in the center, and one antenna in the center of the first chip and the other at the front edge of the second chip.

6.1 Inter-Chip Transmission with Antennas at the Front Edges

The first configuration of interest is placing the antennas at the edge of their respective chips facing towards each other. As shown in section 5.1, placing the antenna at the edge of the chip produced the best directive gain, it's expected that this trend will be seen in the following simulation as well. This configuration was simulated without an AMC, with a partial AMC and with the full AMC for both chips. The HFSS model of the inter chip transmission with antennas at the edge of the chip is shown in Figure 6-1.

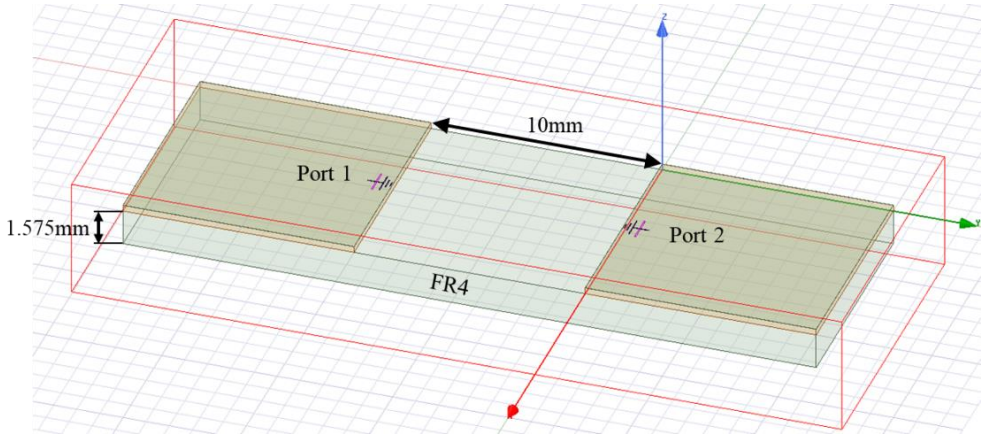

Figure 6-1: Model of Inter-Chip Transmission with Antennas at the front edges without AMC

The two chips in Figure 6-1 are the same as presented previously, Port 1 refers to the antenna on the left and port 2 refers to the antenna on the right. The S_{11} and S_{22} plots are the same because both antennas at port 1 and port 2 are identical. The S_{11} and S_{21} plots are presented in Figure 6-2. The driven element lengths were tuned again to improve the S_{11} plot. The S_{11} and S_{21} plots are presented below.

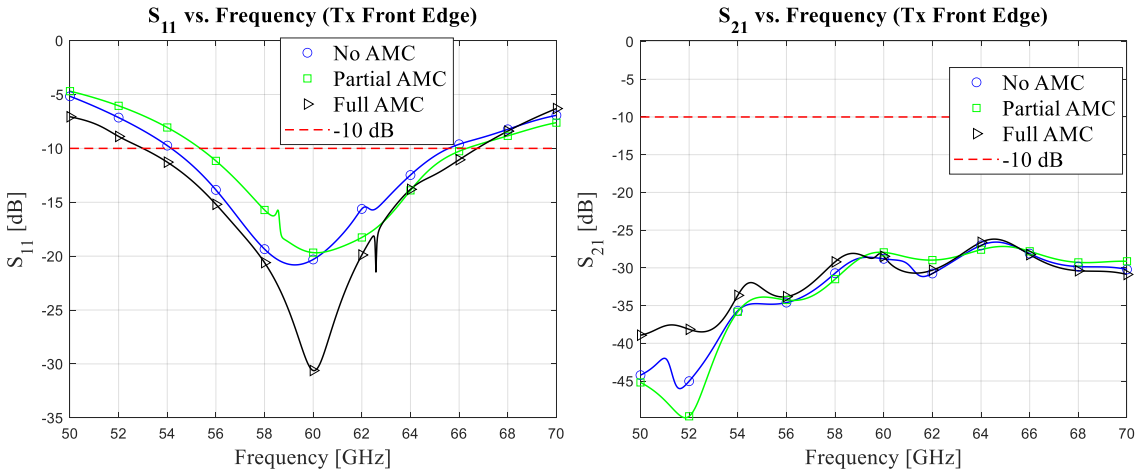

Figure 6-2: S_{11} and S_{21} vs. Frequency plots for Front Edge Transmission.

From the above figure the S_{11} at 60GHz of the antennas with no AMC, a partial AMC and a full AMC are -20.31dB, –19.67 dB, -30.61dB respectively. The 10-dB bandwidths of the antennas with no AMC, partial AMC and Full AMC are 57.02%, 54.76% and 69% of the

V-band respectively. The S_{21} values at 60GHz for the antennas with no AMC, a partial AMC, and a full AMC, are -28.8 dB, -28.0 dB, -28.5 dB respectively. The S_{21} values did not change very much with the addition of the AMC layers. However, all of the configurations performed well with reasonable S_{11} and S_{21} values. The electric field patterns of the three configurations are shown in Figure 6-3 and the 2D radiation patterns from the plane of the chip are in Figure 6-4.

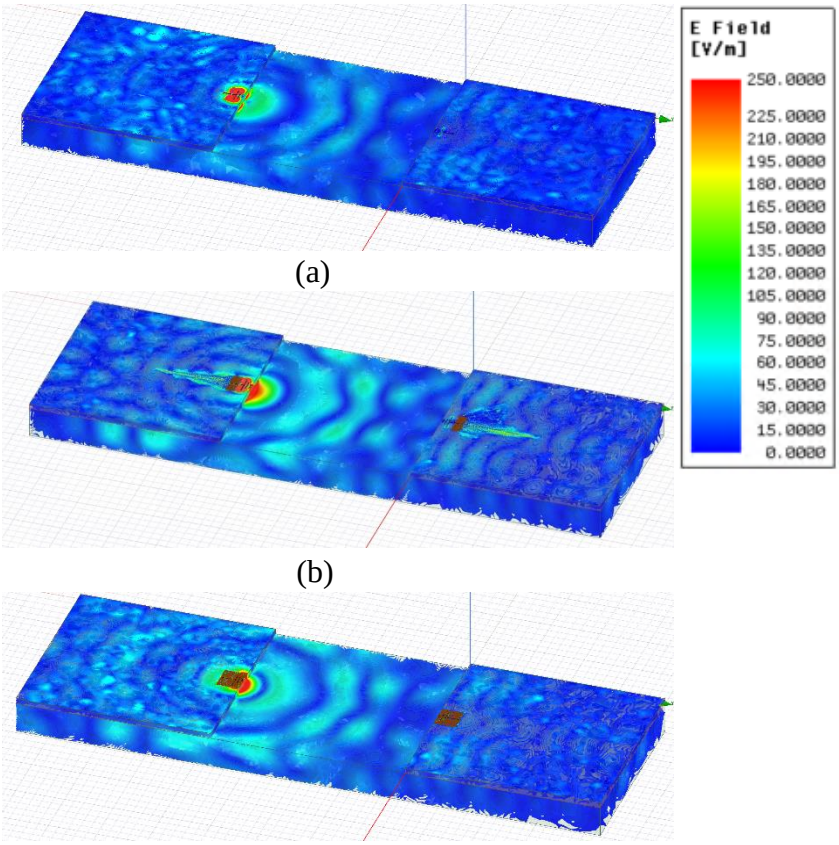

Figure 6-3: E-Field Pattern of Inter-Chip Transmission with Antennas at the front edges and Port 1 excited: No AMC (a), Partial AMC (b), Full AMC (c).

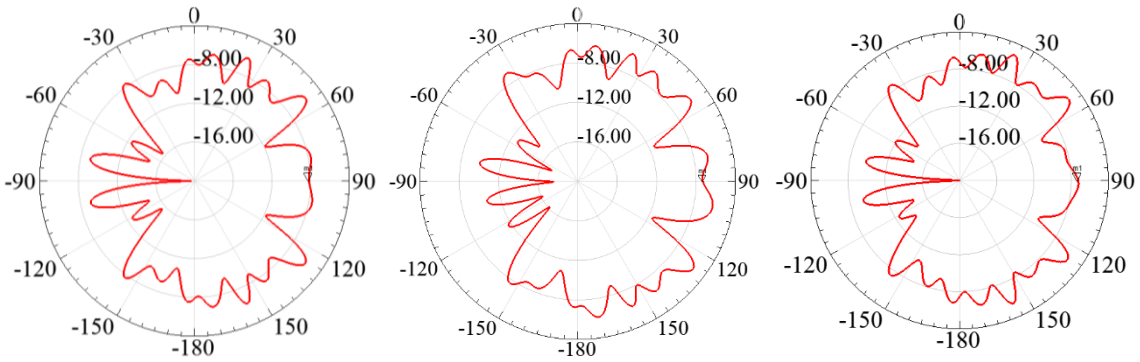

(a) (b) (c)

Figure 6-4: Radiation patterns of Antennas at the front edges with Port 1 excited: No AMC (a), Partial AMC (b), Full AMC (c).

From the E-field patterns in Figure 6-3 the full AMC has the most intense field pattern. Next is the antennas with the partial AMC, and then the antennas without an AMC layer. The directive gains of the configuration without the AMC, with the partial AMC, and with the full AMC are -8.17 dB, -7.31 dB, and -7.24 dB respectively. The radiation efficiency improved from 20.05% without the AMC to 31.13 with the partial AMC, then to 31.84% with the full AMC. Unlike in the single chip shown in section 5.3 it appears that the full AMC performed marginally better than the partial AMC. This is likely because in the transmission configuration the radiation is radiating in the FR4 substrate and not simply in free space. The adjusted director lengths are presented in Table 6-1 along with a summary of the results presented above.

Table 6-1: Summarized results for Inter-Chip Transmission with Antennas at the Front Edge

	Director Length L_2	S_{11} [dB] at 60GHz	S_{21} [dB] at 60GHz	Directive Gain [dB]	Radiation Efficiency	10dB Bandwidth
No AMC	520 µm	-20.31	-28.80	-8.17	20.05%	57.02%
Partial AMC	500 µm	-19.67	-27.95	-7.31	31.13%	54.76%
Full AMC	419 µm	-30.61	-28.47	-7.24	31.84%	68.73%

6.2 Antennas in the Center of the Chips

Next the performance was examined for two chips with Yagi antennas in the center of the them to see how much of an effect the silicon plays on the transmission between them. This configuration was simulated without an AMC, with a partial AMC and with the full AMC for both chips. The HFSS model id shown in Figure 6-5.

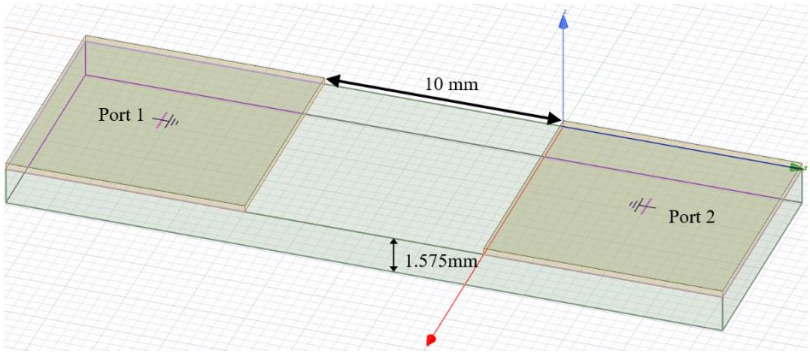

Figure 6-5: Model of Inter-Chip Transmission with antennas in the center

Similar to the last section S_{22} was not plotted because S_{11} and S_{22} are the same. The S_{11} and S_{21} plots of the antennas in Figure 6-5 are sown below.

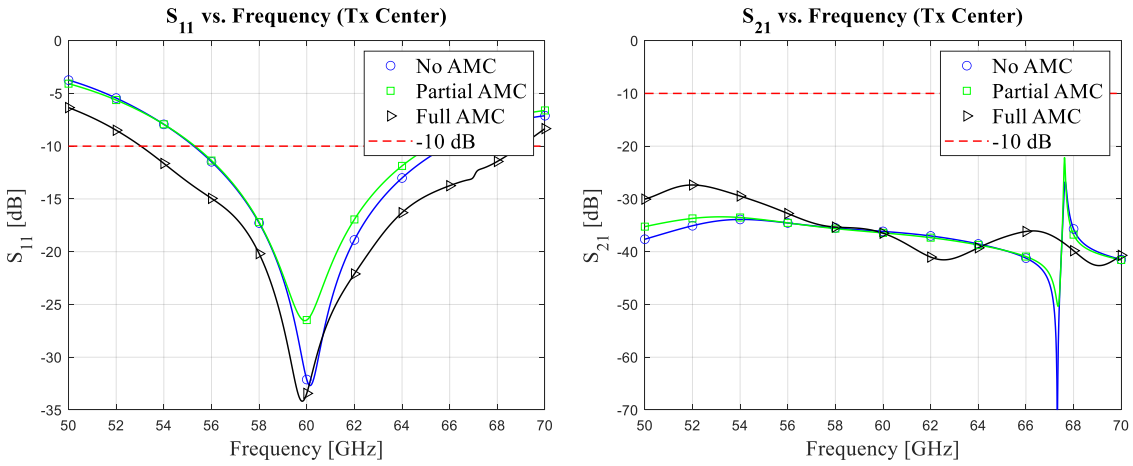

Figure 6-6: S_{11} and S_{21} vs. frequency plots for center to center transmission

From the above figure the S_{11} at 60GHz of the antennas with no AMC, a partial AMC and a full AMC are -32.12 dB, -25.5 dB, -33.43 dB respectively. The 10-dB bandwidths of the

antennas with no AMC, partial AMC and Full AMC are 53%, 56% and 80% of the V-band respectively. The S_{21} values at 60GHz for the antennas with no AMC, a partial AMC, and a full AMC, are -36.16 dB, -36.44 dB, -36.49 dB respectively. The S_{21} values are all effectively the same irrespective of the AMC layers. The full AMC has marginally better S_{11} than the antenna without the AMC and the S_{11} of the partial AMC was considerably worse, but still performs well. The electric field patterns of the three configurations are shown in Figure 6-7 and the 2D radiation patterns from the plane of the chip are in Figure 6-8Figure 6-4.

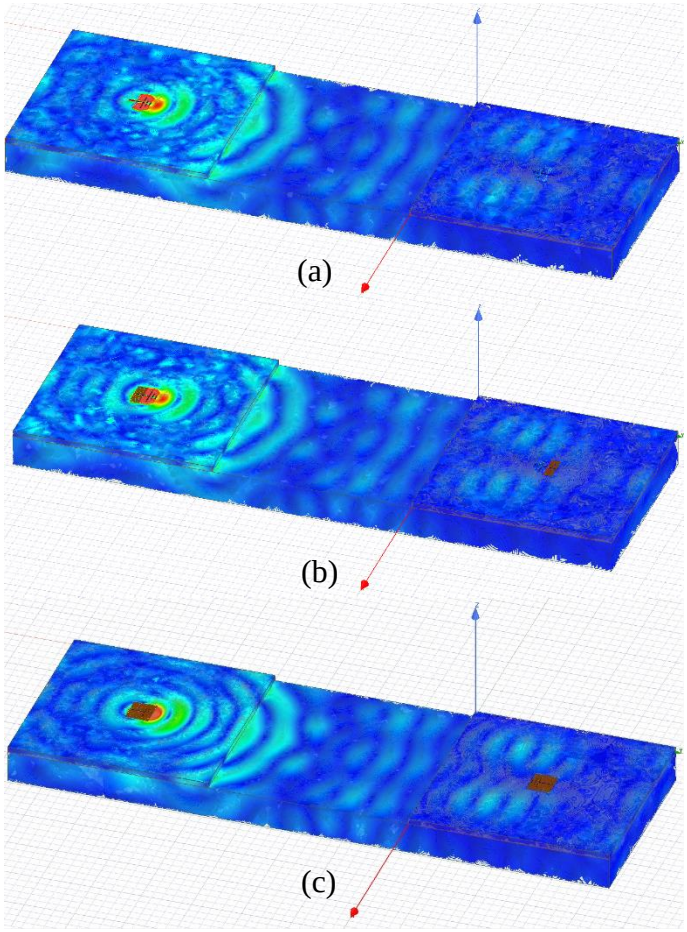

Figure 6-7: E-Field Pattern of Inter-Chip Transmission with Antennas in the Center with port 1 excited: No AMC (a), Partial AMC (b), Full AMC (c).

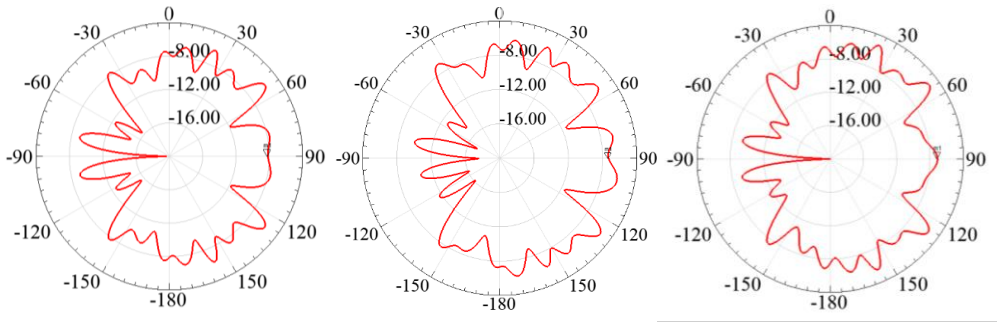

(a) (b) (c)

Figure 6-8: Radiation patterns of antennas in the center of the chips with port 1 excited, (a) No AMC (b) Partial AMC (c) Full AMC.

The E-field patterns shown in Figure 6-7 show more distinctly the distortion in the radiation pattern. The E-Field pattern in all three configurations splits in the center and appears to travel around the antenna in the receiving chip. However, similarly to the last section the E-field pattern is the strongest in the configuration with the full AMCs. The directive gains of the configuration without the AMC, with the partial AMC, and with the full AMC are –5.63 dB, -5.54 dB, and -4.18 dB respectively. The radiation efficiency changed from 15.00% without the AMC to 14.88% with the partial AMC, then to 16.56% with the full AMC. Similarly, to the single chip shown in section 5.2 the full AMC performed better than without an AMC and the partial AMC performed marginally worse. This is for the same reason as discussed in section 5.2. Since the antennas are placed in the center of the chips the silicon impinges on the radiation more and the partial AMC only enhances the radiation behind the antenna. The adjusted director lengths are presented in Table 6-2 along with a summary of the results presented above.

Table 6-2: Summarized results for Inter-Chip Transmission with antennas in the center

	Director Length L_2	S_{11} [dB] at 60GHz	S_{21} [dB] at 60GHz	Directive Gain [dB]	Radiation Efficiency	10dB Bandwidth
No AMC	505 µm	-32.12	-36.16	-5.63	15.00%	53.20%
Partial AMC	501 µm	-25.50	-36.44	-5.54	14.88%	55.56%
Full AMC	405 µm	-33.43	-36.49	-4.18	16.56%	79.74%

6.3 Antennas at the Front Edge and in the Center of the Chips

Next the performance of the antennas placed in the center of the chip and the antennas placed at the front edge of the chips were compared directly in an inter chip configuration. The first chip (port 1) has an antenna placed in the center of the chip and the second chip (port 2) has an antenna placed at the front edge facing the first chip. This configuration was simulated without an AMC, with a partial AMC and with the full AMC for both chips.

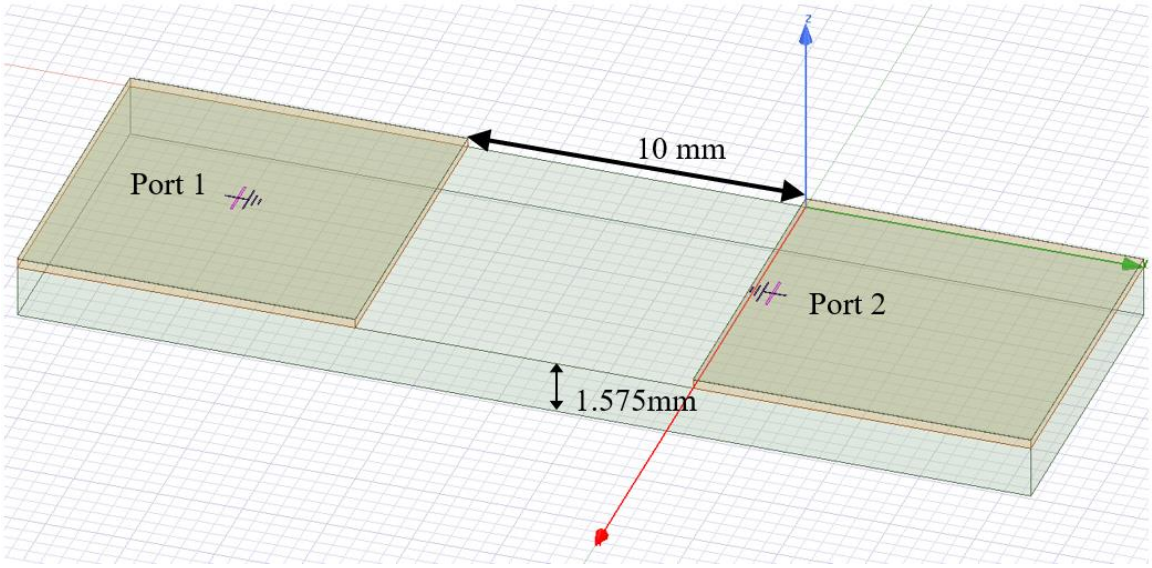

Figure 6-9: Model of Inter-Chip Transmission with antennas in the center and at the edge

The S_{11} performance of these antennas were tuned similarly to the previous configurations by changing the director lengths. The S_{11}, S_{22}, S_{21}, and S_{12} plots are shown in Figure 6-10 and Figure 6-11.

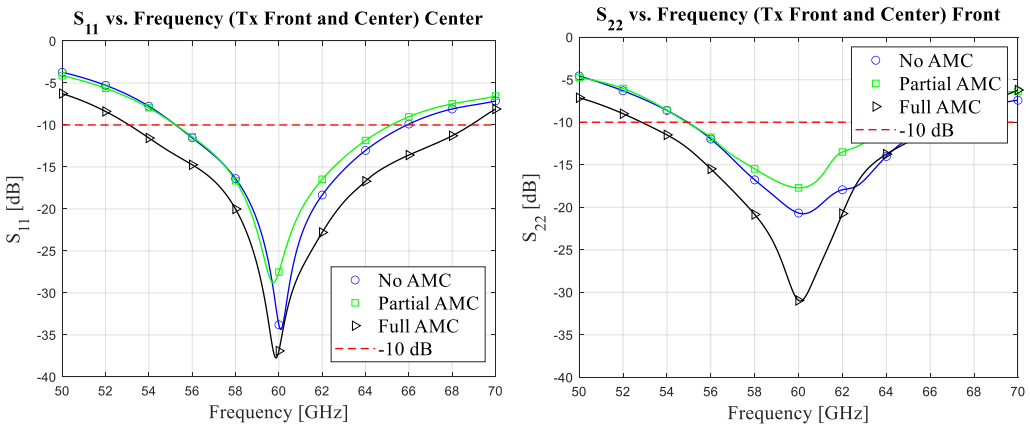

Figure 6-10: S_{11} (left) and S_{22} (right) vs. frequency plots for the center and front antenna placement.

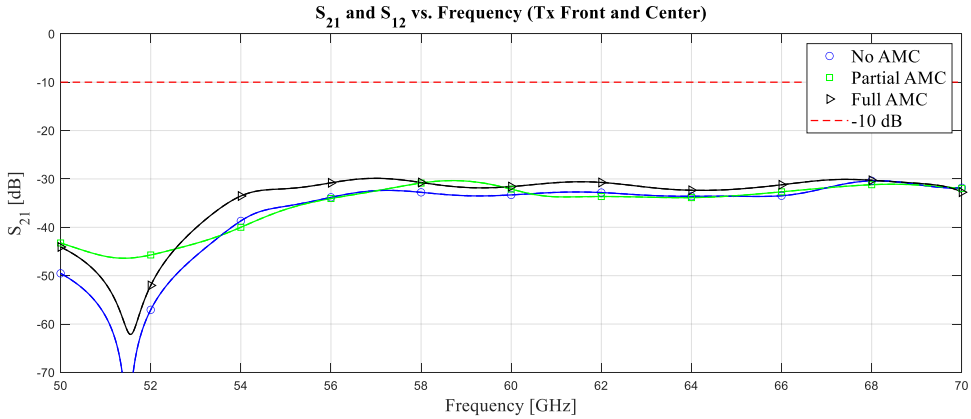

Figure 6-11: S_{21} vs. frequency plot for center and front antenna placement

From the above figures the S_{11} corresponds to the antenna in the center of the chip and the S_{22} corresponds to the antenna at the front edge of the chip. The S_{11} at 60GHz of the antennas with no AMC, a partial AMC and a full AMC are –33.79 dB, -27.51 dB, -36.91 dB respectively. The S_{22} at 60GHz of the antennas with no AMC, a partial AMC and a full AMC are -20.68 dB, -17.72 dB, -30.95 dB respectively. The S_{ii} parameters for the first chip (in the center) had overall better S_{11} than the S_{22} from the chip with the antenna at the front edge. Interestingly the S_{ii} of partial AMC in both cases was worse than without the AMC. For the antenna at the edge the S_{22} significantly improved with the addition of the full AMC. The 10-dB bandwidths of the antennas in the center with no AMC, partial

AMC and Full AMC are 53.3%, 49.7% and 78.8% of the V-band respectively. The 10-dB bandwidths of the antennas at the front edge with no AMC, partial AMC and Full AMC are 57.5%, 48.7% and 69.7% of the V-band respectively. The S_{21} values at 60GHz of the antennas with no AMC, a partial AMC and a full AMC are -33.3 dB, -32.1 dB, -31.58 dB respectively. The S_{21} values are all effectively the same regardless of the AMC layers. These results are all collected in Table 6-3 and Table 6-4. The electric field pattern was plotted for each AMC configuration and with each port excited. These field patterns are all presented in Figure 6-12.

Table 6-3: S-Parameters Measured at 60GHz for Inter-Chip Transmission

	S_{11}[dB] (Center)	S_{22} [dB] (Edge)	S_{21} [dB]
No AMC	-33.79	-20.68	-33.30
Partial AMC	-27.51	-17.72	-32.10
Full AMC	-36.91	-30.95	-31.58

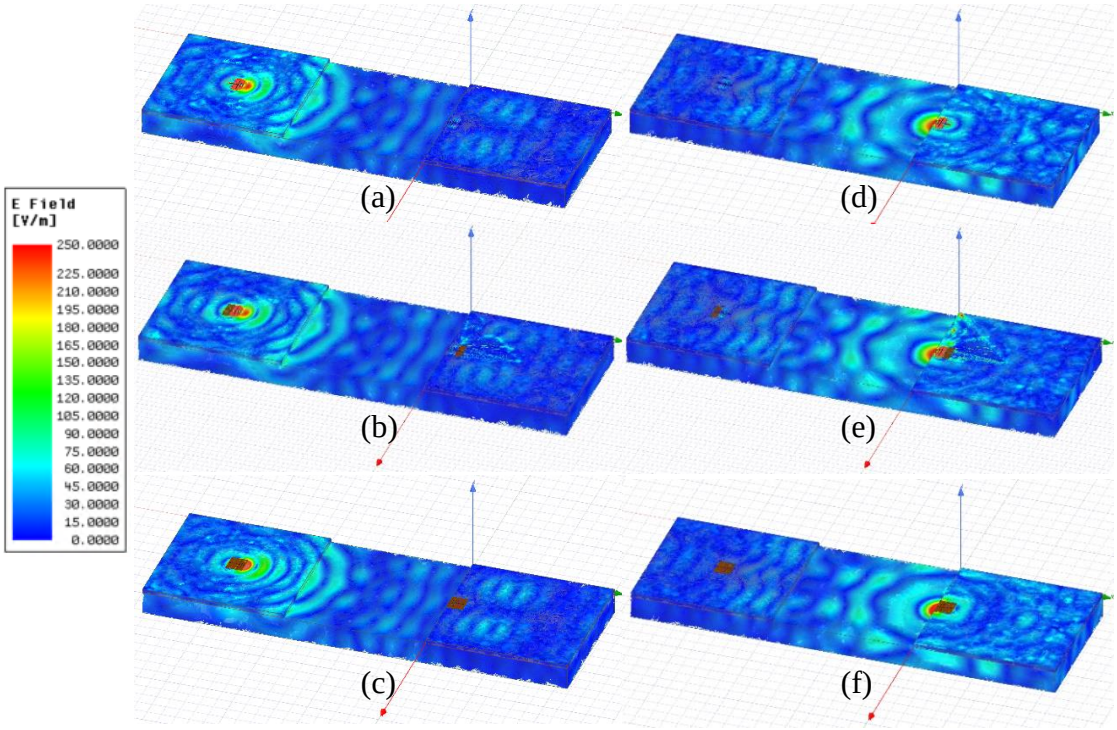

Figure 6-12: E-Field pattern of Inter-Chip Transmission with Antennas in the center and the edge: Port 1 excited No AMC (a), Port 1 excited Partial AMC (b), Port 1 excited Full AMC (c), Port 2 excited No AMC (d), Port 2 excited Partial AMC (e), Port 2 excited Full AMC (f).

Figure 6-12 (a) – (c) show port 1 excited without an AMC, with a partial AMC and with a full AMC. Figure 6-12 (d) – (e) show the same models with port 2 excited. The electric field radiation for models (e) and (f) have the strongest radiation both are improvements to model (d) which has no AMC. Based on inspection Figure 6-12 (e) the model with the Edge antenna energized and a partial AMC appears to have the strongest electric field pattern as it reaches the other antenna. When the antenna on the front edge was energized more electric field ripples reached the antenna at port 1 than when the center antenna was energized. This was as expected because it is travelling in free space for longer before hitting the silicon substrate. The radiation patterns of the six configurations shown in Figure 6-12 are plotted in Figure 6-13 and Figure 6-14.

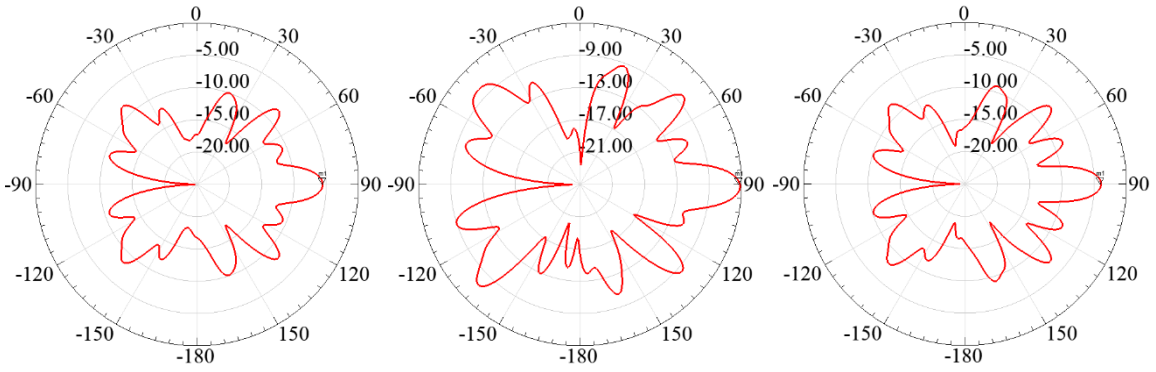

Figure 6-13: Radiation patterns with Port 1 (Center antenna) energized: No AMC (a), Partial AMC (b), Full AMC (c).

Figure 6-13 Shows the radiation patterns for the center antenna without an AMC, with the partial AMC, and with the full AMC. These radiation patterns are from the plane of the chip and straight ahead is at 90˚. The partial AMC has improved the directive gain from -5.54 dB without an AMC to -5.22 with the partial AMC. The full AMC improves the gain to -3.94 dB which is a 29% increase. The radiation efficiency of the antenna decreased by half a percent when the partial AMC was added and improved from 15% without an AMC

to 16.4% when the full AMC was added. The partial AMC improved the gain but reduced the efficiency because the back lobes were also enlarged.

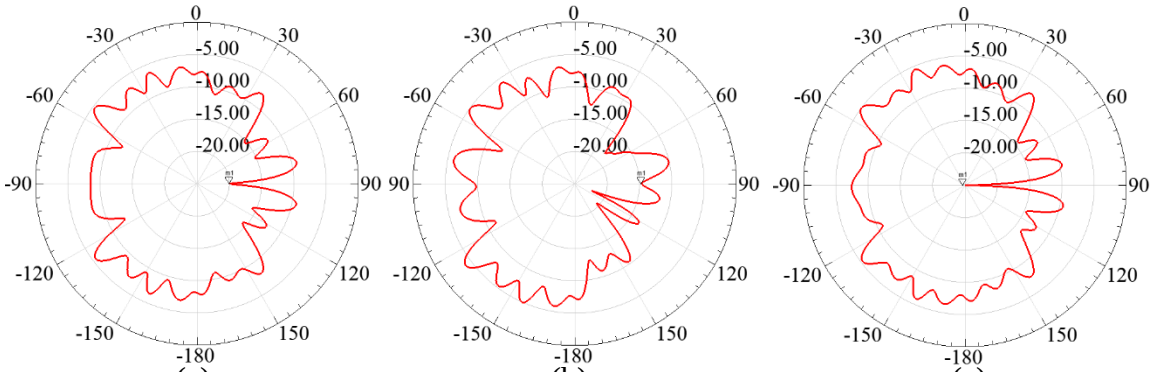

Figure 6-14: Radiation patterns with Port 2 (Edge antenna) energized; No AMC (a), Partial AMC (b), Full AMC (c).

Figure 6-13 shows the radiation patterns of the antenna placed at the front edge of the chip without an AMC, with the partial AMC, and with the full AMC. These radiation patterns are from the plane of the chip and straight ahead is at -90˚. The partial AMC reduced the directive gain from -8.52 dB without an AMC to -9.57 with the partial AMC. While also increasing the radiation efficiency from 29% to 33%. The radiation efficiency of the antenna with the full AMC was only 31.7%, but the directive gain was -7.49 dB. The partial AMC improved the radiation efficiency by reducing the back radiation, while the full AMC improved the directive gain by enhancing the entire signal, however it was not as efficient. These results are presented in Table 6-4.

Table 6-4: Parameters for Antennas at the front and center of the chips in Inter-Chip transmission

		Director Length L_2 [μm]	Directive Gain [dB]	Radiation Efficiency	10dB Bandwidth
Center (Port 1)	No AMC	505	-5.54	15.00%	53.30%
	Partial AMC	501	-5.22	14.50%	49.70%
	Full AMC	403	-3.94	16.40%	78.80%
Front Edge (Port 2)	No AMC	525	-8.52	29.00%	57.50%
	Partial AMC	500	-9.57	33.00%	48.70%
	Full AMC	420	-7.49	31.70%	69.70%

7 Conclusion and Future Work

7.1 Conclusions

The results show that the partial AMC improves the performance of the Yagi antenna when it is placed on the edge of the substrate. The directive gain is enhanced by 46% and the radiation efficiency increased from 39% to 45%. The full AMC layer increases the directive gain (Endfire direction) of the antenna on a small substrate from 0.19 dB to 1.04 dB or 450%. The full AMC also improves the directive gain of the antenna when placed in the center of the larger chip by 5% or 0.93 dB. The full AMC layer improves the directional gain of the antenna in the center of the chip because it is more affected by the silicon substrate, whereas when placed at the edge the antenna is mainly radiating in free space and not as hindered by the lossy silicon. Which is why the partial AMC improves the antenna at the edge. This is more clearly shown by the transmission results. When both antennas were placed at the front edges of their respective chips with full AMC layers the gain increased by 11% and the radiation efficiency increases by 12%; while when both antennas are placed in the center the directive gain increases by 26% and the radiation efficiency increases by only 2%. In the model with one antenna at the front edge of the first chip and the second antenna in the center of the second chip, the full AMC improved the directive gain by 12% for the first chip at the edge and 29% for the second chip in the middle. Both results show that the full AMC has a positive effect on the directive gain of the antenna, especially when placed in the center of the substrate. These results show that adding the full AMC improves the directive gain of the On-chip antennas. If the AMC was extended to cover the entire 10mm by 10mm chip it is expected that the antenna

performance would be even better. The AMC layer was not extended to the entire 10mm by 10 mm chip due to limitations in the available computing cluster. A larger array of AMC unit cells requires more than 300GB of RAM which is more than was available to perform these simulations.

7.2 Future Work

In the future an array of Yagi antennas can be examined in the same CMOS chip to see how the array improves the radiation and gain. The array can be tested with the three AMC layers discussed in the thesis to see their effects on the array. Then the array can be used for beam steering by phasing the array and examining the effects that the AMC layers have on the radiation. The simulations performed in this thesis could also be explored for a larger 20mm by 20mm substrate to see how the larger chip affects the pattern. The AMC could also be used to improve the gain of antennas for intra-chip transmission. If given the opportunity to use a computing cluster with higher computing capabilities the AMC layer could be extended to the entire chip.

8 References

[1] Z. Jia, X. Li, Y. Wang, B. Wang and Y. Chen, "60 GHz millimeter-wave electromagnetic propagation characteristic for inter/intra chip wireless interconnection," in *2013 IEEE International Conference on Signal Processing, Communication and Computing (ICSPCC 2013)*, KunMing, 2013.

[2] R. S. Shelar and M. Patyra, "Impact of Local Interconnects on Timing and Power in a High Performance Microprocessor," *IEEE Transactions on Computer-Aided Design of Integrated Circuits and Systems,* vol. 32, no. 10, pp. 1623-1627, Oct. 2013.

[3] Z. Xiaolai, S. Wei and Z. Wei, "The design and performance analysis of inter-chip wireless communication system in instrument based on 60GHz," in *2015 12th IEEE International Conference on Electronic Measurement & Instruments (ICEMI)*, Qingdao, 2015.

[4] H. Chu, Y. X. Guo, F. Lin and X. Q. Shi, "Wideband 60GHz on-chip antenna with an artificial magnetic conductor," in *2009 IEEE International Symposium on Radio-Frequency Integration Technology (RFIT)*, Singapore, 2009.

[5] Y. Huo, X. Dong and J. Bornemann, "A wideband Artificial Magnetic Conductor Yagi antenna for 60-GHz standard 0.13-µm CMOS applications," *2014 12th IEEE*

International Conference on Solid-State and Integrated Circuit Technology (ICSICT), pp. 1-3, 2014.

[6] C. Z. X. H. Y. Y. T. Liu, "A Low RCS Microstrip Antenna Based on Broadband AMC Structures," in *International Conference on Microwave and Millimeter Wave Technology (ICMMT)*, Chengdu, 2018.

[7] A. A. M. D. a. K. D. F. Mouhouche, "Gain improvement of CPW-Fed monopole antenna over dual-band AMC structure," in *2017 5th International Conference on Electrical Engineering - Boumerdes (ICEE-B)*, Boumerdes, 2017.

[8] M. Iyer, "Compact Antenna with Artificial Magnetic Conductor for Noninvasive Continuous Blood Glucose Monitoring," Rochester Institute of Technology, 2018.

[9] R. Dewan, M. Rahim, M. Hamid, Y. MFM, N. Samsure, N. Murad and K. Kamardin, "Artificial magnetic conductor for var-ious antenna applications: An overview," *International Journal of RF and Microwave Computer-Aided Engineering*, 2017.

[10] M. H. Mehdi Hosseini, "Characteristics Estimation for Jerusalem Cross-Based Artificial Magnetic Conductors," *IEEE Antennas and Wireless Propogation Letters*, vol. 7, pp. 58-61, 2008.